FLOW OF FLUID THROUGH A CURVED TUBE

by

DENIS JOSEPH McCONALOGUE

A thesis submitted to the University of London
for the degree of Doctor of Philosophy
in the Faculty of Science

Centre for Computing and Automation
Imperial College of Science and
Technology

May 1969

Dit is voor Ies, die mij
vier jaar lang aangespoord heeft.

ABSTRACT

Dean's simplified Navier-Stokes equations for the fully-developed flow of a viscous incompressible fluid through a tube of circular cross-section with its axis bent in a circular arc produce a two-dimensional non-linear elliptic equation of the sixth order to be solved in the circular domain. A number of partial-range approximate solutions have been developed, their ranges being expressible in terms of the widely-used non-dimensional parameter

$$k = \frac{2W_m a}{\nu}\sqrt{\frac{a}{L}}$$

where a is the radius of the tube, W_m the mean axial velocity, L the radius of curvature of the axis, and ν the kinematic viscosity. The range $k < 16.6$ has been covered by Dean (1927, 1928) as a perturbation of Poiseuille flow. For $k > 100$, asymptotic solutions have been reported by Adler (1934), Barua (1963) and by Mori and Nakayama (1965). The region $17 < k < 100$ has proved intractable to analytical techniques.

The present thesis gives an exact numerical solution of Dean's equations for $16.6 < k < 77.1$. The first part formulates the method, describes the numerical solution, and provides the results as a set of field plots produced directly by a high-speed computer and associated plotting device. These plots give a complete picture of the progressive change with

increasing k of the flow patterns for the perturbation solution into those for the asymptotic, and in particular, validate for the first time the physical accuracy of the two assumptions on which the asymptotic solutions are based. The second part studies the convective axial dispersion of a substance injected into the tube uniformly over the cross-section, and presents the results in terms of the statistical distribution of mean axial velocity over the injected particles.

The calculated flux ratio is checked against White's (1929) measurements, and the necessary close agreement found.

ACKNOWLEDGMENTS

I wish to acknowledge my deep indebtedness to M.J. Lighthill, Sec. R.S., Royal Society Research Professor Imperial College, with whom I was privileged to collaborate on this problem. Without his invaluable guidance, generously available at all times, the problem would not have been begun or completed.

I wish also to thank my Departmental Head, Professor Stanley Gill, Director of the Centre for Computing and Automation for his interest in the work and his forbearance during the period in which it was completed.

CONTENTS

page

CHAPTER I

CHAPTER I

1. DELIMITATION OF THE PROBLEM

The present thesis is concerned with a limited aspect of the laminar flow of a viscous incompressible fluid through a tube of circular cross-section with its axis bent into a circular arc. Interest is confined to 'fully-developed' flow, which means that the region of flow being examined is sufficiently far downstream from the inlet region for all irregularities to have died out, producing a constant velocity profile over any cross-section. The second limitation has to be expressed in terms of one of the several related non-dimensional parameters on which dynamic similarity can be based, and it is convenient to express it in terms of the widely used

$$k = \frac{2W_m a}{\nu}\sqrt{\frac{a}{L}} \qquad (1)$$

where W_m is the mean axial velocity over the cross-section, a the radius of the tube, ν the kinematic viscosity, and L the radius of curvature of the axis. The solution given in the present thesis covers the range $16.6 < k < 77.1$, a range intermediate between that covered by other theoretical solutions, and in which the physical behaviour of the fluid was hitherto unknown.

2. THE PHYSICAL PROBLEM

Simple physical arguments give a qualitative picture of the flow. The fluid is moving under the action of the pressure in the axial direction, and the centrifugal body forces at right angles to the axis. The axial velocity profile over the cross-section will be a distortion of the paraboloidal profile for Poiseuille flow, but will still be zero at the walls of the tube, and will have its maximum on the central diameter in which the cross-section intersects the plane of the curved axis, and will be symmetrical about this diameter. The body force experienced by any fluid element will be very nearly proportional to the square of its axial velocity (at least for small a/L) so that the fluid near the centre will move in the direction of the centrifugal force, from the inside of the tube (nearer the centre of curvature) to the outside, and the fluid near the walls will be pushed in the opposite direction. By symmetry, the ends of the central diameter are stagnation points, so the overall effect of curvature is to divide the motion of the fluid into two independent regions, symmetrical about the plane of symmetry of the tube, in each of which the fluid particles move in helical paths, the pitch of the helix and the velocity varying from particle to particle.

A quantitative study of the physics of the flow, in particular of the importance of the secondary flow normal to the axis of the tube arising from the centrifugal forces must be based on a solution of an appropriate formulation of the Navier-Stokes equation and the equation of continuity for the system. The formulation is straightforward, but the resulting equations, because of the centrifugal body-force terms which depend on the square of the axial velocity, are non-linear, and insoluble in their full form. The problem is of sufficient physical - and more recently physiological - interest to have stimulated the development of a number of partial range solutions, of which the present is one, and a considerable amount of experimental work.

3. HISTORICAL SURVEY

The first significant theoretical work on the problem was done by Dean (1927) who formulated the full Navier-Stokes equation for the system in a set of toroidal coordinates which were a modification, to cope with curvature, of the natural cylindrical polar coordinates for the straight tube, and simplified these equations by assuming that a/L was so small that the radius of curvature in the centrifugal body-force term could be taken to be constant over the cross-section

of the tube and equal to L; the equations should therefore be physically realistic for small a/L. Dean's equations reduce to a non-linear elliptic equation of the sixth order in two independent variables which has to be solved in the circular domain, and so further simplifications have to be introduced before an approximate analytical solution is possible.

Dean developed a solution of the equations by considering the secondary flow and the change in W, the axial velocity as small perturbations of the known field patterns for Poiseuille flow. This solution enabled him to plot the secondary-flow streamlines, where the secondary-flow streamline of a particular particle is the actual path of the particle in a cross-section which moves axially with the particle; because of the helical motion, these streamlines form two families of closed curves symmetrical about the central diameter (Plots of the secondary-flow streamlines for the intermediate range are given in figure 3, of Chapter II). In an extension of his original solution Dean (1928) showed that dynamic similarity depends on

$$K = \frac{2 W_o^2 a^3}{\nu^2 L} \qquad (2)$$

where W_o is the axial velocity at the centre of the cross-

section, and extended his solution by assuming series expansions in powers of K, inserting these in his equations and comparing powers of K. In spite of the immense work expended on the complex manipulations involved, the results were disappointing, in the sense that predicted departure from Poiseuille flow was small. For example, Dean derived an expression for the ratio of Q_c, the flux ($\pi a^2 W_m$) for a curved tube to Q_s, that for a straight tube with the same pressure gradient, as the first three terms of a power series in K^2; at the upper end of its range of validity K = 576, the expression predicts a drop of less than two percent in the ratio. Dean's work, however, is important, since all subsequent theoretical work on the problem starts from his equations, and his identification of the appropriate parameter for dynamic similarity has provided a common reference for subsequent theoretical and experimental work. His solution covers k in the range (0, 16.6).

White's (1929) experimental measurements of the ratio of γ_s the resistance in a curved pipe to γ_c the resistance in a straight pipe for the same flux Q_s established that dynamic similarity depends on K, though he introduced and used the derived parameter k defined in equation (1). For sufficiently small K,

$$k = \sqrt{K/2} \qquad (3)$$

White's results showed (γ_s / γ_c being equal to Q_c/Q_s) that

Dean's prediction of the virtually constant value of the flux ratio in the range $K < 576$ ($k < 16.6$) was fulfilled. An unexpected discovery from these experiments was that an increase in the curvature ratio increased the value of the Reynolds number below which turbulence is damped out. This aspect was directly examined by Taylor (1929), and the same phenomenon appeared in the work of Adler (1934) who also measured the resistance ratio as a function of k. The work of these three on turbulence is considered briefly and quantitatively in Chapter III, where a comparison of White's measurements with the flux calculations of the numerical solution is also made.

The first asymptotic solution was given by Adler (1934), who deduced that for large K, viscous forces tend to be confined to the boundary, while in the core of the tube, surfaces of equal pressure are perpendicular to the central plane of the tube. By applying a Polhausen analysis to the momentum equations in the boundary layer, he obtained an expression for the increase of the resistance ratio with increasing k. With the same basic assumptions, Barua (1963) and Mori and Nakayama (1965) have given solutions which produce more accurate expressions for the variation of resistance with k. Two relevant questions arise.

The first is whether the upper end of the numerical solution approaches the lower end of the asymptotic, and the second is whether, if the ranges approach, the field patterns and other physical properties are compatible in the region where the solutions impinge. Though an exact lower limit to the asymptotic solutions cannot be given, it can be justifiably claimed that the numerical solution does bridge the gap between the perturbation and asymptotic solutions, since the secondary-flow field patterns it produces at the upper end of the range justify both initial assumptions of the asymptotic solutions. A further indication of the bridging role of the numerical solution is given in the discussion of "median" lengths in Chapter III.

4. THE PRESENT PROBLEM

There is not a great deal of engineering interest in laminar flow through curved tubes with a small curvature ratio (a/L), since relevant flow in curved tubes is usually turbulent, as in heat exchangers, or the curvatures are too sharp or the lengths too small to allow fully-developed flow to occur. However, when the present work was started, it appeared that current investigations into the cardio-vascular system would be greatly helped by a knowledge of the physical behaviour of the fluid flow in the intermediate region

of k, in particular, by a knowledge of the effects of curvature on the dispersion of an injected substance. A further motivation was provided by the local interest in the problem of the Physiological Flow Studies Unit at Imperial College.

It was felt that the present development of computers would make it possible to extend Dean's work upwards by a numerical technique. A number of attempts to solve the problem in the circular cross-sectional region by finite-difference techniques failed because a suitable grid could not be found. A different approach was tried, in which the symmetry of the field patterns about the central diameter could be exploited. The scaled axial velocity w and the scaled secondary-flow stream function ϕ were expressed respectively as cosine and sine Fourier series in the polar angle α measured from the central diameter, with coefficients which are functions of r only, r and α being the natural polar coordinates in the cross-section. After substituting the expressions in the original equations, a set of coupled non-linear ordinary differential equations involving w, ϕ and derived quantities, all functions of r only, were obtained. The problem was discretised, and values of w, ϕ and the other quantities sought by iteration.

It was felt undesirable to base dynamic similarity on a parameter depending on W_m in a theoretical investigation, since W_m is not known even approximately at the outset.

Instead, dynamic similarity was based on a non-dimensional pressure gradient

$$D = \frac{Ga^3}{\mu\nu}\sqrt{\frac{2a}{L}} \qquad (4)$$

where G is the mean pressure gradient.

The iterative method proved to be less convergent than had been anticipated. It started at D = 96 corresponding to Dean's K = 576, and in its original form stopped converging at about D = 140. However, the behaviour of the system suggested that convergence could be forced for higher values of D, and after testing a considerable number of schemes (which have not been chronicled here), one was found which gave convergence up to D = 605.72. The field patterns which had meanwhile emerged showed that no more physical insight would be gained by pushing the value of D higher, since the secondary-flow field patterns at the upper end of the range of D were extremely close to the pattern assumed at the outset of the asymptotic solutions.

Numerical solutions of field problems provide difficulties in interpretation and presentation. With an analytic solution, it is usually possible to see the physical behaviour of the system from the known properties of the functions in which the solution is expressed. In a numerical solution the results are necessarily given as numbers, and this type of interpretation is not possible, though in grid methods,

some insight into the field patterns may be obtained without too much difficulty. The translation of the results of the Fourier-series solution into field patterns by human effort not being feasible, it was decided to make the plotting automatic, so that the field plots would be drawn by an electro-mechanical device, the CALCOMP Plotter, using a magnetic tape produced by the IBM 7094^{II} computer. The flow lines in the numerical solution had to be obtained as a set of discrete points by interpolation along fixed radii. As the plotter could only join these points by straight lines, an algorithm was developed to generate intermediate points on a smooth curve passing through the points. This work was carried on in parallel with the numerical solution of the equations. All the figures in the present thesis, except figure 1 of Chapter II, have been drawn automatically. When the equations had been solved, the flux ratio Q_c / Q_s defined earlier was calculated. This enabled k and D to be correlated, and also made possible a direct test of the numerical solution against White's resistance measurements. Both these are described in Chapter III. This test is crucial since White's measurements are made for small a/L, and Dean's equations are virtually the full Navier-Stokes equations for small a/L, so that a solution which is claimed to be an exact solution of Dean's equations must agree closely with white's well-established measurements.

The extension of the method to the study of the dispersion of an injected substance is given in Chapter III. This has involved the development of algorithms for the evaluation of line integrals around the secondary-flow streamlines, and for calculating the areas enclosed by the streamlines. The developments of these algorithms has necessitated the refinement and sophistication of the algorithms for constructing the streamlines for display, developed in the first part.

The three-dimensional physical picture of dispersion is exceedingly complex, and must be simplified for calculation and presentation. This has been done by restricting interest to the convective axial dispersion of a substance of the same density as the fluid injected as a thin disc uniformly over the cross-section, and by considering only the mean axial velocity of the particles. The statistical distribution of this mean axial velocity over the particles of the injected substance is given in a form which can be used to obtain the downstream axial distribution of the substance at a considerable distance from the site of injection.

Chapter II was published in the Proceedings of the Royal Society, A 307 in 1968. Chapter III is a sequal which is being communicated by Professor M.J. Lighthill, Sec. R.S. for publication in a future issue of the same journal.

Detailed discussion of numerical methods has been confined to the Appendix, where some of the topics of possible interest to other workers in the field are briefly discussed.

References to the work mentioned in this Introduction are given at the end of Chapter III.

CHAPTER II

Proc. Roy. Soc. A. 307, 37–53 (1968)
Printed in Great Britain

Motion of a fluid in a curved tube

By D. J. McConalogue and R. S. Srivastava*
Imperial College, London, S.W. 7

(*Communicated by M. J. Lighthill, Sec.R.S.—Received* 6 *March* 1968)

Dean's work on the steady motion of an incompressible fluid through a curved tube of circular cross-section is extended. A method using a Fourier-series development with respect to the polar angle in the plane of cross-section is formulated and the resulting coupled non-linear equations solved numerically. The results are presented in terms of a single variable $D = 4R\sqrt{(2a/L)}$, where R is the Reynolds number, a the radius of cross-section of the tube, and L the radius of the curve. The results cover the range of D from 96 (the upper limit of Dean's work) to over 600. From these it is found that the secondary flow becomes very appreciable for $D = 600$, moving the position of maximum axial velocity to a distance less than $0{\cdot}38a$ from the outer boundary, and decreasing the flux by 28% of its value for the straight tube.

These calculations fill a large part of the gap in existing knowledge of secondary flow patterns, which lies in the upper range of Reynolds number for which flow is laminar. This range is of particular interest in the investigation of the cardiovascular system.

1. Introduction

In this paper the steady motion of an incompressible fluid through a pipe of circular cross-section which is coiled in a circle has been studied. Dean (1927, 1928) has considered this problem theoretically. He found that, to first approximation (Dean 1927), the relation between pressure gradient and rate of flow is not dependent on the curvature. In order to show its dependence he modified the analysis by including terms of higher order and was able to show (Dean 1928) that the reduction in flow due to curvature depends on a single variable K, equal to $2R^2a/L$, R being the Reynolds number in Dean's notation, a the radius of the tube and L the radius of curvature of the bent tube. Dean (1928) showed that his analysis was reasonably reliable for values of K up to 576. Earlier Dean (1927) had sketched the streamlines in the plane of the cross-section according to his first approximation; these would be accurate only for values of K considerably less than 576. The present investigation has been carried out with a view to finding not only the relation between rate of flow and pressure gradient but more generally the whole pattern of flow for values of $K \geqslant 576$.

Dean mentions that for a complete discussion of possible laminar motions one must have a solution for K up to perhaps 10^5, corresponding to values of a/L around 0·01. The analysis of the present problem has been carried out in such a manner that it depends on a single variable D such that

$$D = \sqrt{\left(\frac{2a^3}{\nu^2 L}\right)}\frac{Ga^2}{\mu},$$

G being the mean pressure gradient, ν being the kinematic viscosity and μ is the

* Permanent address: Defence Science Laboratory, Delhi.

coefficient of viscosity. The D of the problem is related to Dean's K and R by the relation

$$D = 4\sqrt{K} = 4R\sqrt{\frac{2a}{L}}$$

at least for the lower values of K such that mean velocity is related to G approximately as in Poiseuille flow. For higher values, the mean velocity is not known even approximately in advance and so D, expressed in terms of pressure gradient, is a much more convenient parameter than K or R.

Now in a straight tube the lower critical Reynolds number below which all disturbances damp out is approximately 2000. Some experiments conducted by several workers on curved tubes have shown that there is an increase in critical Reynolds number for curved tubes. Taylor (1929) found experimentally that for $L/a = 31{\cdot}9$, the lower critical Reynolds number rose to about 5000. If we substitute in the relation $D = 4R\sqrt{(2a/L)}$, we deduce that values of D up to about 5000 are of interest.

We have solved Dean's equations by an iterative method, and have succeeded in obtaining convergent results for values of D between 96 (which corresponds to Dean's $K = 576$) and 605·72. For several values in this range, the streamlines in the plane of the cross-section have been sketched, clearly demonstrating the character of the secondary flow. Apart from the streamlines in the plane of the cross-section, the lines $w =$ constant have also been sketched, w being the non-dimensional velocity perpendicular to the plane of the cross-section, and these show the very considerable displacement of the location of maximum axial velocity which results from the secondary flow.

In engineering situations, laminar flow rarely occurs because Reynolds numbers are usually too high, and for this reason research on laminar secondary flow has been neglected. But in the cardiovascular system flow is usually laminar. Study of this system (in only parts of which bent tubes occur) makes it desirable, therefore, to investigate laminar secondary flows. Understanding of their streamline patterns can assist, for example, in understanding the distribution of injected substances.

Calculations of such distributions in a bent tube have been attempted by Erdogan & Chatwin (1967), using Dean's solution for small K, but the flow patterns derived in this paper make such an analysis possible for much higher Reynolds numbers, similar to those occurring in the arteries. Such an analysis is now being undertaken.

The gap in existing knowledge has, in fact, been in the upper part of the range of Reynolds numbers for which the flow is laminar. The present paper fills a large part of that gap, and shows that for these Reynolds numbers particularly dramatic changes due to secondary flow occur.

Mathematically, a complicated non-linear elliptic system of the sixth order in two independent variables needs to be solved in a circular domain. A preliminary review of the methods available for doing this indicated that a method using a Fourier-series development with respect to the polar angle had certain advantages. By contrast, methods aimed at determination of function values at points of a grid suffered from the difficulty of choosing a grid ideally suitable for a circular domain.

Finally, the Fourier-series method was chosen, and proved thoroughly convenient for the purpose.

2. Formulation of the problem

Figure 1 shows the system of coordinates for the consideration of motion of fluid through a pipe of circular cross-section coiled in the form of a circle. The axis of the circle in which the pipe is coiled is OZ and C is the centre of the section of the pipe by a plane that makes an angle θ with the fixed axial plane. OC is of length L which is the radius of curvature of the coiled tube. The plane passing through O and perpendicular to OZ will be called the 'central plane' of the pipe, and the circle

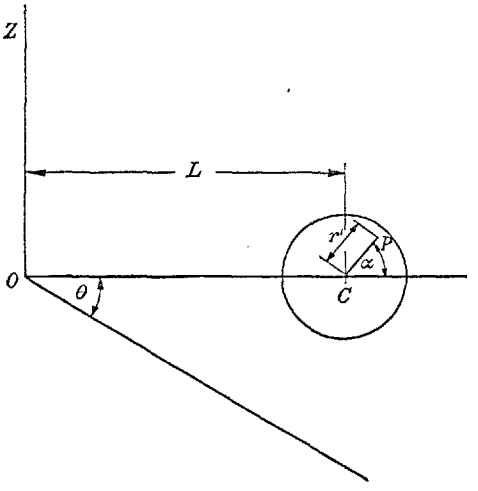

Figure 1

traced out by C its 'central line'. The coordinates of any point P of the cross-section are denoted by the orthogonal coordinates (r', α, θ) where r' is the distance CP and α is the angle which CP makes with the line OC produced. The velocity components corresponding to these coordinates are (U, V, W), U is therefore in the direction CP, V perpendicular to U and in the plane of the cross-section, and W perpendicular to this plane.

The motion of the fluid is supposed to be due to a fall in pressure in the direction of θ increasing. The motion is expected to be a steady one in which U, V, W (but not P, the pressure) are independent of θ.

Dean (1928) obtained simplified equations for such a motion when the curvature of the pipe is small, which means that a/L is small. The equations of motion are

$$U\frac{\partial U}{\partial r'}+\frac{V}{r'}\frac{\partial U}{\partial \alpha}-\frac{V^2}{r'}-\frac{W^2\cos\alpha}{L}=-\frac{\partial}{\partial r'}\left(\frac{P}{\rho}\right)-\frac{\nu}{r'}\frac{\partial}{\partial \alpha}\left(\frac{\partial V}{\partial r'}+\frac{V}{r'}-\frac{1}{r'}\frac{\partial U}{\partial \alpha}\right), \tag{1}$$

$$U\frac{\partial V}{\partial r'}+\frac{V}{r'}\frac{\partial V}{\partial \alpha}+\frac{UV}{r'}+\frac{W^2\sin\alpha}{L}=-\frac{1}{r'}\frac{\partial}{\partial \alpha}\left(\frac{P}{\rho}\right)+\nu\frac{\partial}{\partial r'}\left(\frac{\partial V}{\partial r'}+\frac{V}{r'}-\frac{1}{r'}\frac{\partial U}{\partial \alpha}\right), \tag{2}$$

$$U\frac{\partial W}{\partial r'}+\frac{V}{r'}\frac{\partial W}{\partial \alpha}=-\frac{1}{L}\frac{\partial}{\partial \theta}\left(\frac{P}{\rho}\right)+\nu\left(\frac{\partial^2 W}{\partial r'^2}+\frac{1}{r'}\frac{\partial W}{\partial r'}+\frac{1}{r'^2}\frac{\partial^2 W}{\partial \alpha^2}\right). \tag{3}$$

The equation of continuity is

$$\frac{\partial U}{\partial r'}+\frac{U}{r'}+\frac{1}{r'}\frac{\partial V}{\partial \alpha}=0. \tag{4}$$

These are identical with the equations of motion in cylindrical coordinates r', α and $L\theta$ (the latter replacing z) with the addition of a centrifugal force W^2/L per unit mass acting in the $\alpha = 0$ direction. To this approximation this centrifugal force is the only result of the pipe's curvature.

Now as U, V, W are assumed to be independent of θ, it follows from (3) that P/ρ must be of the form $\theta f_1(r', \alpha)+f_2(r', \alpha)$ and then from (1) and (2) one immediately finds that $f_1(r', \alpha)$ must be a constant. This being so, one can write

$$-\frac{1}{L}\frac{\partial}{\partial \theta}\left(\frac{P}{\rho}\right)=\frac{G}{\rho}, \tag{5}$$

where G is a constant which may be termed the mean pressure gradient; it is equal to the space rate of decrease in pressure along the central line.

From (4) we can write

$$r'U=\frac{\partial f}{\partial \alpha}, \quad V=-\frac{\partial f}{\partial r'} \tag{6}$$

where f, the stream function of the secondary flow, is a function of r' and α only. Now by the use of the equations (1), (2), (3), (5) and (6) one obtains the following two equations

$$\left(-\frac{\partial f}{\partial \alpha}\frac{\partial}{\partial r'}+\frac{\partial f}{\partial r'}\frac{\partial}{\partial \alpha}\right)\nabla_1^2 f+\frac{2W}{L}\left(r'\sin\alpha\frac{\partial W}{\partial r'}+\cos\alpha\frac{\partial W}{\partial \alpha}\right)=-\nu r'\nabla_1^4 f \tag{7}$$

and

$$\frac{1}{r'}\left(-\frac{\partial f}{\partial r'}\frac{\partial W}{\partial \alpha}+\frac{\partial f}{\partial \alpha}\frac{\partial W}{\partial r'}\right)=\frac{G}{\rho}+\nu\nabla_1^2 W \tag{8}$$

where

$$\nabla_1^2=\frac{\partial^2}{\partial r'^2}+\frac{1}{r'}\frac{\partial}{\partial r'}+\frac{1}{r'^2}\frac{\partial^2}{\partial \alpha^2}.$$

Now introducing the non-dimensional variables

$$f=\nu\phi, \quad W=\sqrt{\left(\frac{\nu^2 L}{2a^3}\right)}\,w, \quad r'=ar \tag{9}$$

we obtain

$$\nabla_1^2 w+D=\frac{1}{r}\left(\frac{\partial \phi}{\partial \alpha}\frac{\partial w}{\partial r}-\frac{\partial \phi}{\partial r}\frac{\partial w}{\partial \alpha}\right) \tag{10}$$

and

$$-\nabla_1^4\phi=\left(\frac{\partial \phi}{\partial r}\frac{1}{r}\frac{\partial}{\partial \alpha}-\frac{1}{r}\frac{\partial \phi}{\partial \alpha}\frac{\partial}{\partial r}\right)\nabla_1^2\phi+w\left(\sin\alpha\frac{\partial w}{\partial r}+\frac{\cos\alpha}{r}\frac{\partial w}{\partial \alpha}\right) \tag{11}$$

where

$$D=\frac{Ga^2}{\mu}\sqrt{\frac{2a^3}{\nu^2 L}}.$$

In the equations (10) and (11) ∇_1^2 stands for

$$\frac{\partial^2}{\partial r^2}+\frac{1}{r}\frac{\partial}{\partial r}+\frac{1}{r^2}\frac{\partial^2}{\partial \alpha^2}.$$

3. We now introduce the series

$$w = \sum_{n=0}^{\infty} w_n \cos n\alpha \tag{12}$$

and

$$\phi = \sum_{n=0}^{\infty} \phi_n \sin n\alpha, \tag{13}$$

where w_n and ϕ_n are functions of r only.

Substituting w from equation (12) in equation (10) and by equating the coefficients of $\cos n\alpha$, the following equations are obtained. For $n = 0$, we obtain

$$\frac{\mathrm{d}^2 w_0}{\mathrm{d}r^2} + \frac{1}{r}\frac{\mathrm{d}w_0}{\mathrm{d}r} = f_0(r), \tag{14}$$

where

$$f_0(r) = \frac{1}{2r}\left[\sum_{m=1}^{\infty} m\phi_m \frac{\mathrm{d}w_m}{\mathrm{d}r} + \sum_{m=1}^{\infty} m w_m \frac{\mathrm{d}\phi_m}{\mathrm{d}r}\right] - D. \tag{15}$$

For $n \geqslant 1$, we have

$$\frac{\mathrm{d}^2 w_n}{\mathrm{d}r^2} + \frac{1}{r}\frac{\mathrm{d}w_n}{\mathrm{d}r} - \frac{n^2}{r^2} w_n = f_n(r), \tag{16}$$

where

$$f_n(r) = \frac{1}{2r}\sum_{m=-\infty}^{\infty} m\phi_m \frac{\mathrm{d}s_{n-m}}{\mathrm{d}r} - \frac{1}{r}\sum_{m=-\infty}^{\infty} m s_m \frac{\mathrm{d}\phi_{n-m}}{\mathrm{d}r}. \tag{17}$$

In equations (16) and (17) we have used the following relations

$$\left.\begin{aligned} \phi_{-m} &= -\phi_m, \\ s_m &= w_m \quad (m > 0), \\ s_m &= w_{-m} \quad (m < 0), \\ s_0 &= 2w_0. \end{aligned}\right\} \tag{18}$$

If we now introduce the vorticity ζ', then from (6) we have

$$\frac{\partial^2 f}{\partial r'^2} + \frac{1}{r'}\frac{\partial f}{\partial r'} + \frac{1}{r'^2}\frac{\partial^2 f}{\partial \alpha^2} = \zeta'. \tag{19}$$

With $\zeta' = \zeta(\nu/a^2)$ (where ζ is non-dimensional vorticity), by the use of (9) we obtain

$$\frac{\partial^2 \phi}{\partial r^2} + \frac{1}{r}\frac{\partial \phi}{\partial r} + \frac{1}{r^2}\frac{\partial^2 \phi}{\partial \alpha^2} = \zeta. \tag{20}$$

Here

$$\zeta = \sum_{n=0}^{\infty} \zeta_n \sin n\alpha, \tag{21}$$

ζ_n being a function of r only, satisfying

$$\frac{\mathrm{d}^2 \phi_n}{\mathrm{d}r^2} + \frac{1}{r}\frac{\mathrm{d}\phi_n}{\mathrm{d}r} - \frac{n^2}{r^2}\phi_n = \zeta_n. \tag{22}$$

Now substituting ϕ from (13) in (11) and equating the coefficients of $\sin n\alpha$, one obtains for $n \geqslant 1$

$$\frac{\mathrm{d}^2 \zeta_n}{\mathrm{d}r^2} + \frac{1}{r}\frac{\mathrm{d}\zeta_n}{\mathrm{d}r} - \frac{n^2}{r^2}\zeta_n = F_n(r), \tag{23}$$

where

$$\begin{aligned} F_n(r) = &-\frac{1}{r}\sum_{m=-\infty}^{\infty} m\zeta_m \frac{\mathrm{d}\phi_{n-m}}{\mathrm{d}r} + \frac{1}{r}\sum_{m=-\infty}^{\infty} m\phi_m \frac{\mathrm{d}\zeta_{n-m}}{\mathrm{d}r} \\ &- \frac{1}{4}\sum_{m=-\infty}^{\infty} \frac{\mathrm{d}s_m}{\mathrm{d}r}(s_{n-(m+1)} - s_{n-(m-1)}) + \frac{1}{4r}\sum_{m=-\infty}^{\infty} m s_m (s_{n-(m+1)} + s_{n-(m-1)}). \end{aligned} \tag{24}$$

In equation (24), in addition to the relations given by (18) we have $\zeta_{-m} = -\zeta_m$.

4. Solution

By the application of the method of variation of parameters (Jeffreys & Jeffreys 1962) one obtains from (14)

$$w_0 = A + B\ln r + \int_u^r \xi(\ln r - \ln \xi) f_0(\xi)\,d\xi, \tag{25}$$

where A and B are constants and u may be taken arbitrarily.

Now the velocity W has to be finite at $r = 0$ which implies that w_n has to be regular at $r = 0$ for all $n \geqslant 0$.

At $r = 0$, therefore we would have

$$w_0 \sim B\ln r + \ln r \int_u^0 \xi f_0(\xi)\,d\xi$$

which gives

$$B = -\int_u^0 \xi f_0(\xi)\,d\xi.$$

The velocity W is zero at the boundary and so we get $w_n = 0$ at $r = 1$. The condition $w_0 = 0$ at $r = 1$ therefore from (25) gives

$$A = \int_u^1 (\xi \ln \xi) f_0(\xi)\,d\xi.$$

Finally, from (25) we obtain

$$w_0 = \int_r^1 (\xi \ln \xi) f_0(\xi)\,d\xi + \ln r \int_0^r \xi f_0(\xi)\,d\xi. \tag{26}$$

Again from (17) we get

$$w_n = Ar^n + Br^{-n} + \frac{1}{2n}\int_u^r (r^n \xi^{-n+1} - r^{-n}\xi^{n+1}) f_n(\xi)\,d\xi. \tag{27}$$

The conditions on w_n determine A and B. They are

$$A = \frac{1}{2n}\int_0^1 \xi^{n+1} f_n(\xi)\,d\xi - \frac{1}{2n}\int_u^1 \xi^{-n+1} f_n(\xi)\,d\xi$$

and

$$B = \frac{1}{2n}\int_u^0 \xi^{n+1} f_n(\xi)\,d\xi.$$

Finally, we have

$$w_n = \frac{r^n}{2n}\int_0^1 \xi^{n+1} f_n(\xi)\,d\xi + \frac{r^n}{2n}\int_1^r \xi^{-n+1} f_n(\xi)\,d\xi - \frac{r^{-n}}{2n}\int_0^r \xi^{n+1} f_n(\xi)\,d\xi. \tag{28}$$

Again from (23) we obtain

$$\phi_n = Ar^n + Br^{-n} + Cr^{n+2} + Dr^{-n+2} + \frac{1}{8n}\left[\int_u^r \frac{\xi^{n+1} r^{-n+2} - r^n \xi^{-n+3}}{n-1} F_n(\xi)\,d\xi \right.$$
$$\left. + \int_u^r \frac{\xi^{-n+1} r^{n+2} - r^{-n}\xi^{n+3}}{n+1} F_n(\xi)\,d\xi\right] \tag{29}$$

where A, B, C, and D are constants. Now ϕ_n is regular at $r = 0$. Therefore we should have

$$B = \frac{1}{8n}\int_u^0 \frac{\xi^{n+3}}{n+1} F_n(\xi)\,d\xi \quad \text{and} \quad D = -\frac{1}{8n}\int_u^0 \frac{\xi^{n+1}}{n-1} F_n(\xi)\,d\xi.$$

At $r = 1$, U and V both are zero. This boundary condition therefore gives $\phi_n = 0$ and $\phi_n = 0$ at $r = 1$. This determines A and C. After A and C have been determined we obtain from (29) for $n \geqslant 2$

$$\begin{aligned}\phi_n = {} & r^n\left[\frac{1}{8n}\int_0^1 \xi^{n+3} F_n(\xi)\,d\xi - \frac{1}{8}\int_0^1 \frac{\xi^{n+1} F_n(\xi)}{n-1}\,d\xi\right] \\ & + r^{n+2}\left[\frac{1}{8n}\int_0^1 \xi^{n+1} F_n(\xi)\,d\xi - \frac{1}{8}\int_0^1 \frac{\xi^{n+3} F_n(\xi)}{n+1}\,d\xi\right] \\ & - \frac{r^{-n}}{8n}\int_0^r \frac{\xi^{n+3} F_n(\xi)}{n+1}\,d\xi + \frac{r^{-n+2}}{8n}\int_0^r \frac{\xi^{n+1} F_n(\xi)}{n-1}\,d\xi \\ & - \frac{r^n}{8n}\int_1^r \frac{\xi^{-n+3} F_n(\xi)}{n-1}\,d\xi + \frac{r^{n+2}}{8n}\int_1^r \frac{\xi^{-n+1} F_n(\xi)}{n+1}\,d\xi. \end{aligned} \tag{30}$$

For $n = 1$, one obtains from (23)

$$\begin{aligned}\phi_1 = {} & Ar^3 + \frac{B}{r} + C(r\ln r) + Dr + \frac{r^3}{16}\int_u^r F_1(\xi)\,d\xi - \frac{1}{16r}\int_u^r \xi^4 F_1(\xi)\,d\xi \\ & - \frac{(r\ln r)}{4}\int_u^r \xi^2 F_1(\xi)\,d\xi + \frac{r}{4}\int_u^r (\xi^2 \ln \xi) F_1(\xi)\,d\xi. \end{aligned} \tag{31}$$

After applying the conditions on ϕ_1, we get

$$\begin{aligned}\phi_1 = {} & \frac{r^3}{16}\int_0^1 (2\xi^2 - \xi^4) F_1(\xi)\,d\xi + \frac{r}{8}\int_0^1 (\xi^4 - \xi^2) F_1(\xi)\,d\xi \\ & + \frac{r^3}{16}\int_1^r F_1(\xi)\,d\xi - \frac{1}{16r}\int_0^r \xi^4 F_1(\xi)\,d\xi - \frac{r\ln r}{4}\int_0^r \xi^2 F_1(\xi)\,d\xi \\ & + \frac{r}{4}\int_1^r (\xi^2 \ln \xi) F_1(\xi)\,d\xi. \end{aligned} \tag{32}$$

Now by using the equations (22) and (30) one obtains

$$\begin{aligned}\zeta_n = {} & \frac{(n+1)r^n}{2n}\int_0^1 \xi^{n+1} F_n(\xi)\,d\xi - \frac{r^n}{2n}\int_0^1 \xi^{n+3} F_n(\xi)\,d\xi \\ & + \frac{r^n}{2n}\int_1^r \xi^{-n+1} F_n(\xi)\,d\xi - \frac{r^{-n}}{2}\int_0^r \xi^{n+1} F_n(\xi)\,d\xi. \end{aligned} \tag{33}$$

For numerical purposes it is easiest to use (33) to obtain ζ_n directly, and then to deduce ϕ_n from (22) in the same manner as w_n was obtained from (16), namely as

$$\phi_n = \frac{r^n}{2n}\int_1^r \xi^{-n+1}\zeta_n(\xi)\,d\xi - \frac{r^{-n}}{2n}\int_0^r \xi^{n+1}\zeta_n(\xi)\,d\xi \tag{34}$$

using the fact that

$$\int_0^1 \xi^{n+1}\zeta_n(\xi)\,d\xi = 0,$$

which can be established directly from equation (33).

The equations (33) and (34) are true for $n \geqslant 1$. We also need the following results for derivatives:

$$\frac{\mathrm{d}w_0}{\mathrm{d}r} = \frac{1}{r}\int_0^r \xi f_0(\xi)\,\mathrm{d}\xi, \tag{35}$$

$$\frac{\mathrm{d}w_n}{\mathrm{d}r} = \frac{r^{n-1}}{2}\int_0^1 \xi^{n+1} f_n(\xi)\,\mathrm{d}\xi + \frac{r^{n-1}}{2}\int_1^r \xi^{-n+1} f_n(\xi)\,\mathrm{d}\xi + \frac{r^{-n-1}}{2}\int_0^r \xi^{n+1} f_n(\xi)\,\mathrm{d}\xi, \tag{36}$$

$$\frac{\mathrm{d}\zeta_n}{\mathrm{d}r} = \frac{(n+1)r^{n-1}}{2}\int_0^1 \xi^{n+1} F_n(\xi)\,\mathrm{d}\xi - \frac{nr^{n-1}}{2}\int_0^1 \xi^{n+3} F_n(\xi)\,\mathrm{d}\xi + \frac{r^{n-1}}{2}\int_1^r \xi^{-n+1} F_n(\xi)\,\mathrm{d}\xi + \frac{r^{-n-1}}{2}\int_0^r \xi^{n+1} F_n(\xi)\,\mathrm{d}\xi, \tag{37}$$

$$\frac{\mathrm{d}\phi_n}{\mathrm{d}r} = \frac{r^{n-1}}{2}\int_1^r \xi^{-n+1}\zeta_n(\xi)\,\mathrm{d}\xi + \frac{r^{-n-1}}{2}\int_0^r \xi^{n+1}\zeta_n(\xi)\,\mathrm{d}\xi. \tag{38}$$

At $r = 0$ our formulae take the special forms:

$$(w_0)_0 = \int_0^1 \xi \ln \xi f_0(\xi)\,\mathrm{d}\xi, \tag{39}$$

$$(w_n)_0 = 0 \quad (n \geqslant 1), \tag{40}$$

$$\left(\frac{\mathrm{d}w_0}{\mathrm{d}r}\right)_0 = 0, \tag{41}$$

$$\left(\frac{\mathrm{d}w_1}{\mathrm{d}r}\right)_0 = \frac{1}{2}\int_0^1 (\xi^2 - 1) f_1(\xi)\,\mathrm{d}\xi, \tag{42}$$

$$\left(\frac{\mathrm{d}w_n}{\mathrm{d}r}\right)_0 = 0 \quad (n \geqslant 2), \tag{43}$$

$$(\phi_n)_0 = 0 \quad (n \geqslant 1), \tag{44}$$

$$\left(\frac{\mathrm{d}\phi_1}{\mathrm{d}r}\right)_0 = -\frac{1}{2}\int_0^1 \zeta_1(\xi)\,\mathrm{d}\xi, \tag{45}$$

$$\left(\frac{\mathrm{d}\phi_n}{\mathrm{d}r}\right)_0 = 0 \quad (n \geqslant 2), \tag{46}$$

$$(\zeta_n)_0 = 0 \quad (n \geqslant 1), \tag{47}$$

$$\left(\frac{\mathrm{d}\zeta_1}{\mathrm{d}r}\right)_0 = \int_0^1 \xi^2 F_1(\xi)\,\mathrm{d}\xi - \frac{1}{2}\int_0^1 (\xi^4 + 1) F_1(\xi)\,\mathrm{d}\xi, \tag{48}$$

$$\left(\frac{\mathrm{d}\zeta_n}{\mathrm{d}r}\right)_0 = 0 \quad (n \geqslant 2), \tag{49}$$

$$(f_0)_0 = \left(\frac{\mathrm{d}\phi_1}{\mathrm{d}r}\right)_0 \left(\frac{\mathrm{d}w_1}{\mathrm{d}r}\right)_0 - D, \tag{50}$$

$$(f_n)_0 = 0 \quad (n \geqslant 1) \tag{51}$$

$$(F_n)_0 = 0 \quad (n \geqslant 1). \tag{52}$$

The flux across any cross-section is given by

$$\begin{aligned} Q_c &= \int_0^a \int_0^{2\pi} W r' \, \mathrm{d}r' \, \mathrm{d}\alpha \\ &= \sqrt{\left(\frac{\nu^2 L}{2a^3}\right)} \int_0^a \int_0^{2\pi} \left(\sum_{n=0}^{\infty} w_n \cos n\alpha \right) r' \, \mathrm{d}r' \, \mathrm{d}\alpha \\ &= 2\pi a^2 \sqrt{\left(\frac{\nu^2 L}{2a^3}\right)} \int_0^1 r w_0 \, \mathrm{d}r. \end{aligned}$$

Now if Q_s denotes the flux in a straight tube for the same pressure gradient as that in a curved tube, then we have

$$\frac{Q_c}{Q_s} = \frac{16}{D} \int_0^1 r w_0 \, \mathrm{d}r. \tag{53}$$

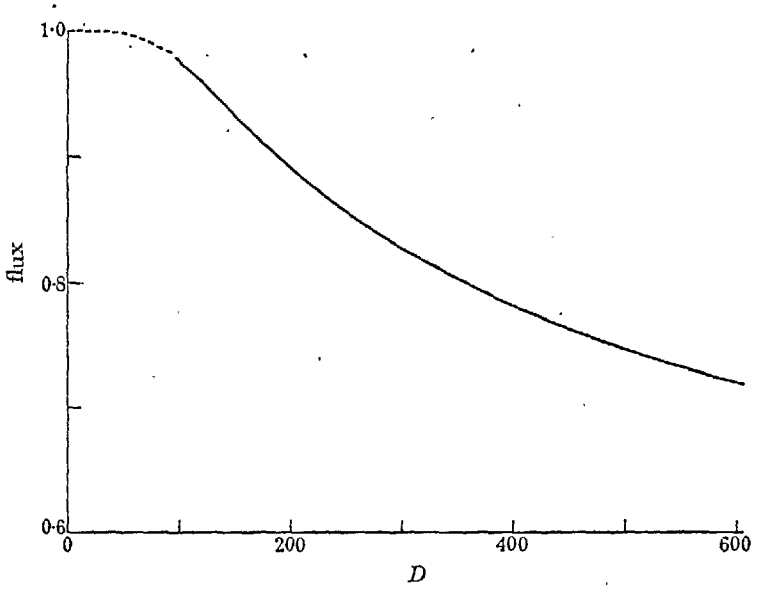

FIGURE 2

NUMERICAL SOLUTION

The equations (26), (28) and (33) to (38) express w_n, ϕ_n and ζ_n and their derivatives in terms of $f_n(\xi)$ and $F_n(\xi)$, which are, in turn, defined in terms of w_n, ϕ_n and ζ_n and their derivatives in equations (15), (17) and (24). This has been done because it is not possible to obtain analytical expressions for w and ϕ. In consequence, numerical values for their Fourier coefficients defined in equations (12) and (13), corresponding to particular values of D are sought by numerical iteration, using the equations just listed.

Since numerical techniques cannot cope with functions defined at every point in a continuous range, w, ϕ and their related functions must be replaced by discretized representations. For the present numerical work, the range (0, 1) has been divided into ten equal parts, so that each function is replaced by a vector whose elements

correspond to the eleven values of the function at $\xi = 0(0{\cdot}1)1$. It will be convenient to denote the vector analogue of any function v by a bold face v, and the elements of v by v_s, $s = 0(1)10$.

To solve the discrete analogue of the original problem, a process must be devised, which, starting from a set of approximations to $\mathbf{w}_n$, $\boldsymbol{\varphi}_n$ and $\boldsymbol{\zeta}_n$, and the related derivatives, uses the known relationships between them to get an improved set of approximations. The process is applied repeatedly to each successive set of approximations, until convergence, which is taken to have occurred when a set of approximations has been obtained, on which the application of the iterative process produces changes which are less than a chosen tolerance. This implies that a mutually consistent set of vectors has been obtained.

Evaluation of the integrals

Before any iterative scheme can be devised, a method must be developed for evaluating the integrals occurring in equations (26), (28) and (34) to (38), in which the integrand is of the general form $p(\xi)f(\xi)$, where $p(\xi)$ is one of the continuously defined weighting functions $\xi \ln \xi$, ξ^{n+1}, ξ^{-n+1} $(n = 1, 2, \ldots)$ but $f(\xi)$ has been replaced by the vector **f**. To derive quadrature formulae, **f** must be replaced (implicitly or explicitly) by a continuously defined approximating function, for which it is customary to use a collocating polynomial. For each $p(\xi)$, the range $(0, 1)$ may be covered in increments of $0{\cdot}1$, by a set of two-panel formulae (generalizations of Simpson's rule) of the form

$$\int_{s/10}^{(s+2)/10} p(\xi)f(\xi)\,\mathrm{d}\xi = A_0 f_s + A_1 f_{s+1} + A_2 f_{s+2} + E \quad (s = 0(1)8), \tag{54}$$

E being an error term, with special one-panel formulae for $(0, 0{\cdot}1)$ and $(0{\cdot}9, 1)$. In (54), $f(\xi)$ is replaced by a quadratic over the range of integration, so E will only be zero when $f(\xi)$ is a polynomial of degree two or less, and the piece-wise approximation will lead to discontinuities in the integral. The A's depend on $p(\xi)$ and s, but not on $f(\xi)$, and this can be used to obtain their numerical values from the three simultaneous equations which arise by making (54) exact when $f(\xi)$ is taken as 1, ξ and ξ^2 in turn (the method of undetermined coefficients). The different triplets of A's corresponding to each $p(\xi)$ need be worked out once only, outside the iteration loop.

This approach was used initially, but was found to give increasingly inaccurate results for $p(\xi) = \xi^{-n+1}$, with increasing n and decreasing ξ. It was not usable for $n > 6$.

Because of the form of the weighting functions, and because the method of piece-wise collocation gives rise to discontinuities in the integrals, there are obvious advantages in replacing **f** by a single polynomial covering the whole range $(0, 1)$. The integrations can then be carried out analytically. The unique polynomial of degree ten passing through $(0{\cdot}1s, f_s)$ would not be a suitable choice, since its value could oscillate unrealistically between the collocation points, and while the error due to this oscillation would tend to cancel out with unit weighting function and integration extending over the entire range, the partial-range integration combined

with the steeply varying weighting functions would amplify any error due to spurious oscillation.

It was decided to approximate f by a least-squares polynomial, the degree of which would be determined by numerical experimentation, as the best compromise between the need to minimize unwanted oscillation, and the need to represent f with sufficient accuracy.

Since the least-squares approximation has to be done repeatedly, it becomes computationally economical to carry it out in terms of the Gram polynomials (Hildebrand 1956), the discrete analogues of the Legendre polynomials. The relevant set is the set $\{\phi_r(s, 10)\}$, where $\phi_r(s, 10)$ is a polynomial of degree r in s, and the members are orthogonal under summation, i.e.

$$\sum_{s=0}^{10} \phi_r(s, 10)\,\phi_m(s, 10) = \gamma_r \delta_{rm}. \tag{55}$$

The least-squares polynomial of degree q is given by

$$\left.\begin{aligned} p_q(\xi) &= \sum_{r=0}^{a} a_r \phi_r(10\xi, 10) \quad (q \leqslant 10), \\ \text{where} \qquad a_r &= \frac{1}{\gamma_r} \sum_{s=0}^{10} f_s \phi_r(s, 10), \\ \gamma_r &= \sum_{s=0}^{10} \phi_r^2(s, 10). \end{aligned}\right\} \tag{56}$$

Considerable algebraic manipulation is necessary to derive the polynomials in s, and to transform them into polynomials in ξ. The actual computing time, however, for each least-squares approximation is very short, since the values of $\phi_r(s, 10)$ at $s = 0(1)10$ can be stored initially as a set of eleven element vectors; a_r is then obtained as the inner product of two eleven element vectors, divided by a constant γ_r, also calculated once only.

A polynomial of degree eight was found suitable, and used throughout the investigation. It is expected that w_n and ϕ_n would decrease very rapidly with increasing n, so only the first few terms in the infinite summations in equations (15), (17) and (24) contribute significantly to the values of the sum. The computer program made provision for twelve terms, and this was found more than adequate.

Iterative schemes

By increasing the parameter D in steps, initial approximations to w_n, $\boldsymbol{\phi}_n$ and derived quantities for a particular value of D are provided by the final iterated values of the corresponding quantities for the immediately lower value of D. The process was started from $D = 96$, which corresponds to Dean's $K = 576$.

For this value of D, the first approximation to w_0 from (26) is

$$w_0 = \tfrac{1}{4}D(1-r^2).$$

The first approximation to ϕ_1, from equation (31) is then

$$\phi_1 = (\tfrac{1}{4}D)^2 \tfrac{1}{576}(-r^7 + 6r^5 - 9r^3 + 4r).$$

For w_1, equation (28) gives

$$w_1 = (\tfrac{1}{4}D)^3 \tfrac{1}{576}(\tfrac{19}{40}r - r^3 + \tfrac{3}{4}r^5 - \tfrac{1}{4}r^7 + \tfrac{1}{40}r^9).$$

By the use of equation (22), an approximation is obtained to ζ_1, and differentiation gives approximations to the corresponding derivatives.

For the subsequent discussion, it is convenient to use the symbols $\mathbf{v}_I^{(k)}$ and $\mathbf{v}_F^{(k)}$ to distinguish between the initial and final approximations to the vector $\mathbf{v}$ in the kth iteration.

In each iteration, n gives from 0 to 11. In the kth iteration, for $n = 0$, equations (11) and (49) use $\mathbf{w}_{mI}^{(k)}$, $\boldsymbol{\phi}_{mI}^{(k)}$ and their derivatives to calculate $\mathbf{f}_0$, which is then used in equations (26) and (40), and (35) and (41) to obtain $\mathbf{w}_{0F}^{(k)}$ and $(\mathbf{dw}_0/\mathbf{dr})_F^{(k)}$. A choice is now available between using $\mathbf{w}_{0F}^{(k)}$ or $\mathbf{w}_{0I}^{(k)}$ (and their respective derivatives) in the subsequent calculations with $n \geqslant 1$; more generally, the choice is between incorporating new values immediately, or continuing with the old values until the end of iteration (analogously to the Gauss–Seidel and Jacobi processes for the iterative solution of linear simultaneous equations). Experience with both methods shows unambiguously that the new values should be used as soon as they become available.

At the outset, the straightforward iterative scheme

$$\mathbf{v}_I^{(k+1)} = \mathbf{v}_F^{(k)}$$

was used for all the vectors, and D, starting at 96, was increased by a factor of $10^{0\cdot1}$ ($= 1\cdot259$). It is, of course, necessary for any iterative scheme (unless it is highly convergent), that the initial approximations should be reasonably close to the final converged values.

The straightforward scheme worked well for $D = 96$, but became more slowly convergent for increasing D, and finally became divergent. Since the convergence depends on the initial approximations, it is not practicable or necessary to fix a precise value of D at which it breaks down, especially as the results of this part of the work showed several properties of the behaviour of the system which could be used to increase the value of D for which convergence could be obtained.

The convergence or divergence of the system was dominated by the behaviour of $\mathbf{w}_0$. Also the effect of the iterative scheme was to make the values oscillate, whether convergent or divergent. Accordingly, a better result could be expected by taking

$$\mathbf{v}_I^{(k+1)} = \tfrac{1}{2}(\mathbf{v}_I^{(k)} + \mathbf{v}_F^{(k)})$$

for all the vectors. This increased the rate of convergence for the previous convergent values of D, and extended the value of D for which convergence was obtained, but again began to give oscillatory values, and was found to be non-convergent for values of D around 260, even starting from a good approximation. A new approximation was tried in which $\mathbf{v}_I^{(k+1)}$ was the average of all the previous means, i.e.

$$\mathbf{v}_I^{(k+1)} = \frac{1}{2k}\sum_{r=1}^{k}(\mathbf{v}_I^{(r)} + \mathbf{v}_F^{(r)}).$$

Because of the oscillatory effect of the iterative process, this scheme could be expected to be stable and self-correcting. This was indeed borne out in practice, but

the scheme was not pushed to its limits, because the convergence was somewhat slow, i.e. $\mathbf{v}_I^{(k)}$ and $\mathbf{v}_F^{(k)}$ approached rather slowly. As this was seen to be due to the continuing influence of the values for the lower values of k, the rate of convergence could be increased by weighting the later mean values more heavily according to the scheme

$$\mathbf{v}_I^{(k+1)} = \sum_{r=1}^{k} S_r(\mathbf{v}_I^{(r)} + \mathbf{v}_F^{(r)})/2 \sum_{r=1}^{k} S_r$$

where $\{S_r\}$ is a monotonic increasing sequence, whose actual form is not of primary importance; a typical useful form was $S_r = 1 + (r/12)^4$. This scheme would be convergent for all values of D for which $\mathbf{v}_I^{(k)}$ and $\mathbf{v}_F^{(k)}$ tended to a common limit with increasing k, for all the vectors.

Above $D = 380$, exponential incrementing of D had to be replaced by arithmetic incrementation, 25 being found to be a suitable increment between 380 and 480, and 10 between 480 and 605.

Results

Figure 2 gives the plot of flux against D for values of D up to 605·72. The dotted line is a plot of Dean's formula for the flux,

$$1 - \left(\frac{K}{576}\right)^2 (0{\cdot}03058) + \left(\frac{K}{576}\right)^4 (0{\cdot}01159)$$

and the continuous line from $D = 96$ is a plot of twenty-eight values obtained in the present work by evaluating the integral in equation (53).

In figure 3 *a–i*, level surfaces of ϕ = constant and w = constant have been plotted for nine values of D in a geometric progression whose first term is 96 and common ratio $10^{0{\cdot}1}$. For w, ten lines have been drawn, the constant increment being $w_{\max.}/11$, where $w_{\max.}$ is the maximum value of w, found by interpolation along the diameter $\alpha = 0$, and for ϕ, eight dotted lines with increments $\phi_{\max.}/9$, $\phi_{\max.}$ being the maximum value of ϕ, found also by interpolation. The position of $w_{\max.}$ is also indicated on each graph.

Figures 2 and 3 have been drawn mechanically on a CALCOMP Plotter, using a magnetic tape produced by the Imperial College IBM 7090 computer. When the iterative procedure had converged for a particular value of D, the values of w at the twenty-one equally spaced points along a set of diameters 3° apart, were calculated by summing the Fourier series (12) at each point. The points along the grid lines corresponding to w = constant were obtained by direct cubic interpolation, giving a set of points lying on a closed curve. These were joined using a special computer routine which enabled the CALCOMP Plotter to pass a smooth curve through them, having a continuous slope.

The curves for ϕ = constant were similarly obtained, except that ϕ was defined at eleven equally spaced points along the radii.

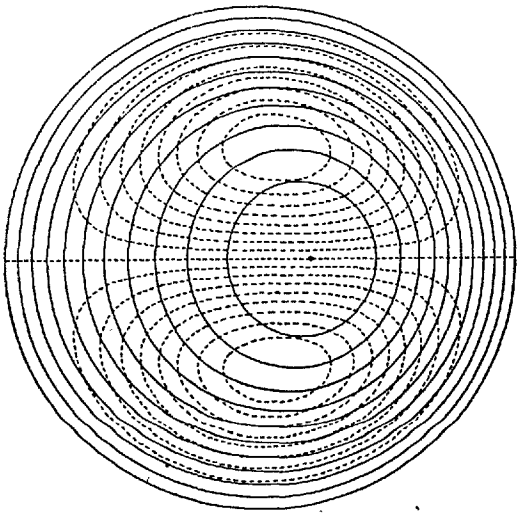

(a)

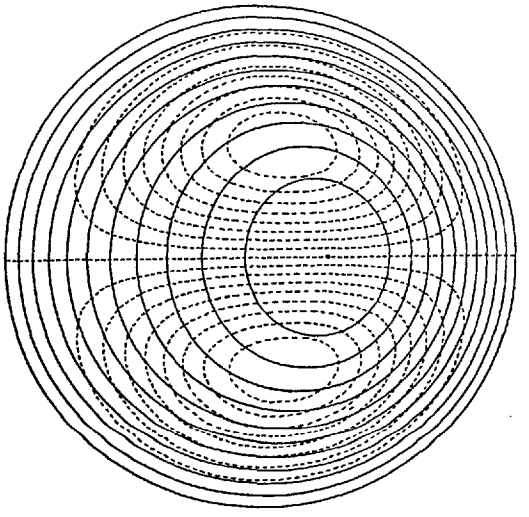

(b)

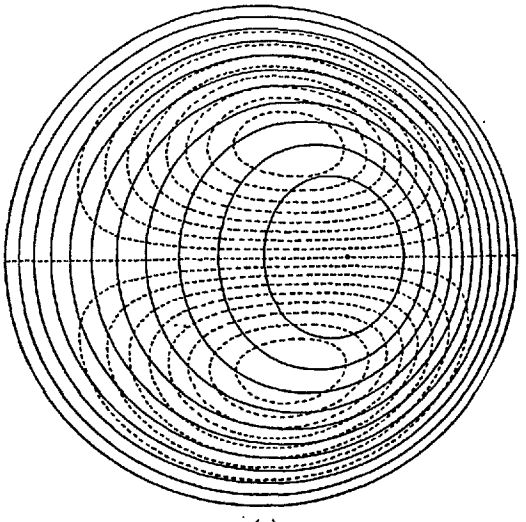

(c)

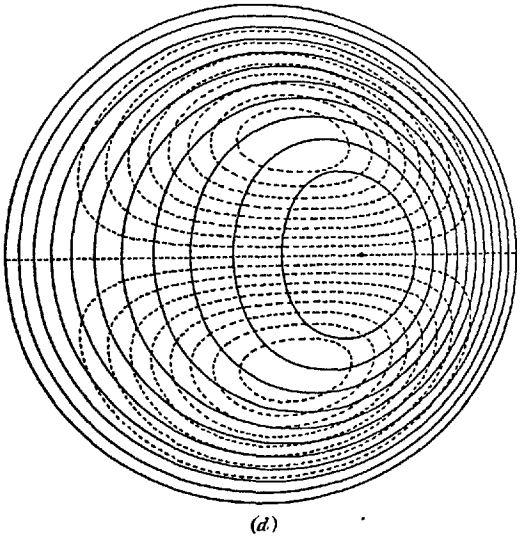

(d)

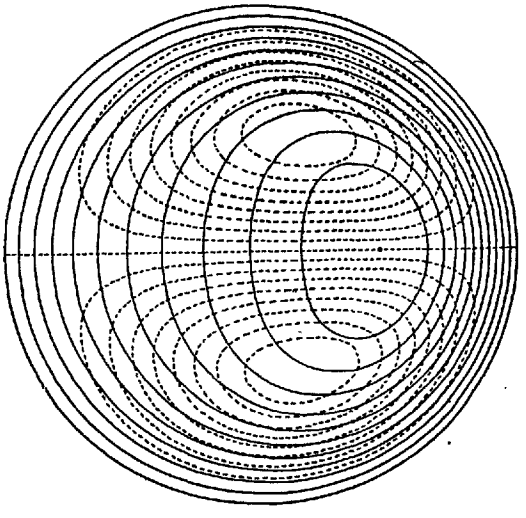

(e)

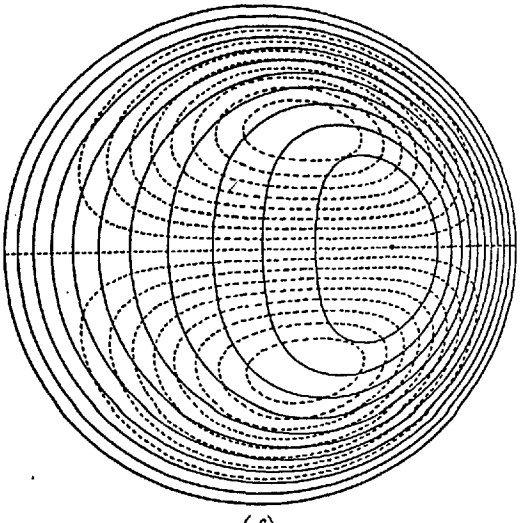

(f)

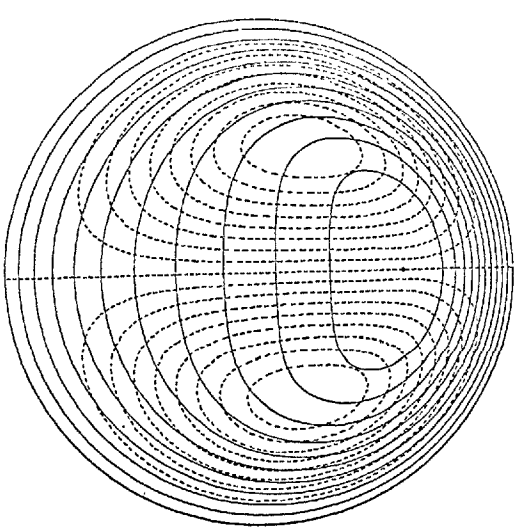

(*g*)

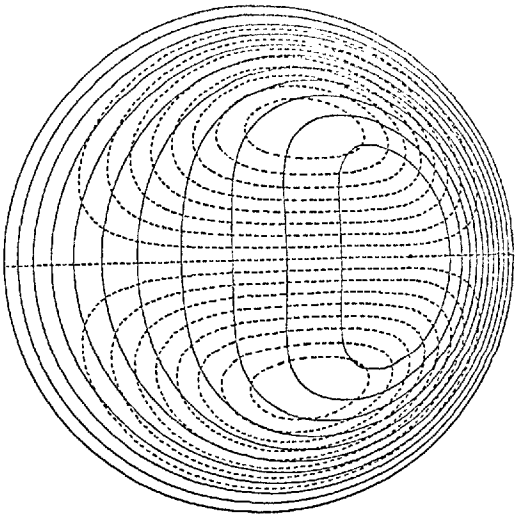

(*h*)

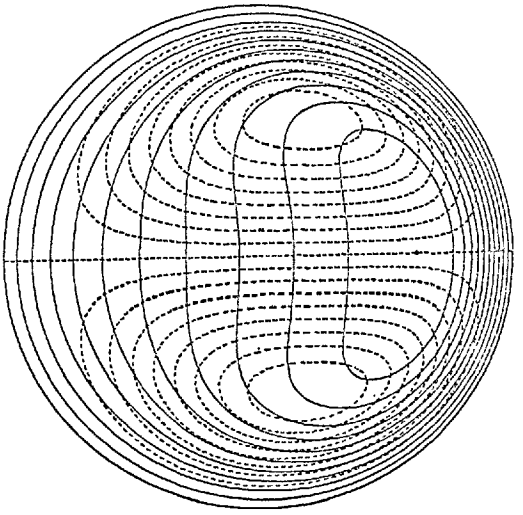

(*i*)

FIGURE 3

	D	$W_{\max.}$	$\phi_{\max.}$
a	96	23·4	0·95
b	120·86	28·8	1·36
c	152·15	35·0	1·85
d	191·55	42·2	2·42
e	241·14	50·5	3·08
f	303·58	60·0	3·83
g	382·18	71·3	4·69
h	481·14	83·9	5·71
i	605·72	98·5	6·81

Physical discussion of results

The pattern of streamlines of the secondary flow in the plane of the cross-section that Dean (1927) obtained for small D was symmetrical between the inside and the outside of the bend. It could be thought of as driven by a distribution of centrifugal force which is a maximum in the centre of the cross-section (where for small D the axial velocity is greatest) and falls to zero at the walls.

For larger values of the pressure-gradient parameter D, however, the secondary flow has convected the axial-momentum peak well away from the centre of the cross-section, as figures 3*a–i* show. Accordingly, the distribution of the centrifugal force which drives the secondary flow itself is no longer symmetrical; the centrifugal force takes much greater values on the outside of the bend. The secondary-flow streamlines are, accordingly, not symmetrical between the inside and outside of the bend, and indeed, their form shows that secondary-flow velocity components take much greater values on the outside of the bend.

The streamline patterns for large D show, furthermore, that a gradient of pressure (between high pressure on the outside of the bend and low on the inside) so opposes this distribution of centrifugal force that in a large central region of the tube cross-section the secondary-flow velocity is approximately uniform. This central region of approximately uniform secondary flow is a particularly interesting and unexpected result of the computations.

Approximately the same pressure gradient acts near the wall (far from the plane of symmetry) where centrifugal force is much lower, to accelerate further the secondary flow, which attains its highest speeds on this part of the circuit, while returning towards the inside of the bend. This, however, is a region where viscous forces are, no doubt, effective in restraining further build-up of secondary-flow velocities.

It is not surprising that within the central region of approximately uniform secondary flow there is a subregion where the lines of constant axial velocity w indicate a uniform gradient of w (increasing towards the outside of the bend). This subregion is far from the walls of the tube, and viscous forces may be small there, in which case the constant axial pressure gradient must produce an approximately constant axial acceleration. If x is a Cartesian coordinate in the plane of the cross-section, pointing towards the outside of the bend, and the secondary flow has an x-component of velocity approximately constant and equal to U, then this axial acceleration is approximately $U(\partial w/\partial x)$, so that its approximate constancy in a central subregion would imply approximately uniform gradient $\partial w/\partial x$ in thatregion.

Finally, the movement of the axial velocity peak nearer the wall increases the viscous rate of dissipation due to shear, and so for given axial pressure gradient there is a considerably reduced flux Q_c in the curved tube compared with the value Q_s for a straight tube. Figure 2 shows that, where D has reached the value 600, the ratio Q_c/Q_s has already fallen to 0·721. All these results confirm that secondary flow produces very big effects at the higher Reynolds numbers for which laminar flow is to be expected.

The authors are extremely grateful to Professor M. J. Lighthill, Sec. R.S., Royal Society Research Professor for suggesting the problem and for his invaluable suggestions and continued guidance in the course of preparation of this paper. One of us (R. S. S.) expresses his sincere thanks to the Royal Society for awarding a Post Doctoral Research Assistantship for the period during which this work was completed.

References

Dean, W. R. 1927 *Phil. Mag.* 4, 208.
Dean, W. R. 1928 *Phil. Mag.* 5, 673.
Erdogan, M. E. & Chatwin, P. C. 1967 *J. Fluid Mech.* 29, 465.
Jeffreys, H. & Jeffreys, B. S. 1962 *Methods of mathematical physics* (3rd ed.), p. 494. Cambridge University Press.
Hildebrand, F. B. 1956 *Introduction to numerical analysis*, p. 290. New York: McGraw-Hill.
Taylor, G. I. 1929 *Proc. Roy. Soc.* A 124, 243.

CHAPTER III

The Effects of Secondary Flow on the Laminar Dispersion of an Injected Substance in a Curved Tube

by

D.J. McConalogue

Imperial College, London S.W.7

ABSTRACT

The numerical solution by McConalogue and Srivastava (1968) of Dean's simplified Navier-Stokes equations for the laminar flow of an inviscid fluid through a tube of circular cross-section of radius a, coiled in a circular arc of radius L, and valid for k in the range (16.6, 77.1), where $k = R\sqrt{\frac{a}{L}}$, R the Reynolds number, is compared with experiment, correlated to the asymptotic solutions for $k > 100$, and extended to study the convective axial dispersion of a substance injected into the tube. The variation of the calculated flux ratio agrees closely with White's (1929) measurements of the inverse quantity over the same range, and the field patterns for the upper end of the range establish the validity of the two basic assumptions of the asymptotic solutions. The original method is extended to calculate the mean axial velocity of a typical particle of the fluid and to present the statistical distribution

of mean velocity over the particles of a substance injected as a thin disc uniformly over the cross-section of the tube. These distributions are used to display the variation with k of the shape of indicator concentration-time curves. The anticipated effect of secondary flow, in producing a more uniform distribution of velocity over the fluid than in Poiseuille flow, is evident.

1. INTRODUCTION

The iterative Fourier-series solution of Dean 's (1927) simplified Navier-Stokes equations for the laminar flow of an incompressible viscous fluid through a curved tube of circular cross-section given by McConalogue and Srivastava (1968) is extended in the present paper to calculate the effects of the secondary flow on the dispersion of a substance injected into the tube. As a preliminary to this extension, the validity of the numerical solution is tested, directly by comparing its results with experiment, and indirectly by relating its results to theoretical work for a higher range of the dimensionless parameter on which dynamic similarity is based.

The numerical solution was made to depend on a single varaible D, a non-dimensional pressure gradient defined by

$$D = \frac{Ga^3}{\mu\nu}\sqrt{\frac{2a}{L}} \qquad (1)$$

where G is the mean axial pressure gradient, a the radius of the tube, L the radius of curvature of its axis, μ the viscosity and ν the kinematic viscosity. Convergent solutions were obtained for D in the range (96, 605.72), a region intermediate between the ranges covered by the perturbation solution of Dean (1927, 1928) and the asymptotic solutions of Barua (1963), and Mori and Nakayama (1965). The numerical solution starts at D = 96, the top of the range for which Dean's series solution is valid, and the straightforward relationship of the two solutions has been adequately treated in the previous paper. The relationship to the asymptotic solutions is discussed here.

The numerical solution predicts the variation of flux ratio with D, flux ratio being defined as the ratio of Q_c, the flow through a curved tube to Q_s, the flow through a straight tube for the same pressure gradient. This prediction is tested against White's (1929) experimental measurements of the reciprocal quantity over the same range of D.

In White's work and in the asymptotic solutions, dynamic similarity is based on k, defined by

$$k = \frac{2aW_m}{\nu}\sqrt{\frac{a}{L}} \qquad (2)$$

where W_m is the mean velocity of flow in the axial direction, and in experimental work is obtained from the flux which is directly measured. In theoretical work, W_m is known only when the distribution of W over the cross-section has been obtained, so k and D have to be related through the flux calculations.

Letting

$$\frac{Q_c}{Q_s} = f(D) \qquad (3)$$

and using Poiseuille's formula,

$$Q_s = \frac{\pi G a^4}{8\mu} \qquad (4)$$

it follows that

$$W_m = \frac{Q_c}{\pi a^2} = \frac{Ga^2}{8\mu} f(D) \qquad (5)$$

or, using equations (1) and (2)

$$Df(D) = 4\sqrt{2k} \qquad (6)$$

The corresponding values of D and k are given in table 1.

Table 1

	D	k	W_{max}
a	96.00	16.60	18.95
b	128.86	20.47	23.19
c	152.15	25.03	28.23
d	191.55	30.39	34.04
e	241.14	36.75	40.83

f	303.58	44.32	48.79
g	382.18	53.35	58.25
h	481.14	64.10	69.45
i	605.72	77.05	82.62

Using Dean's results, together with the twenty-eight values of the flux ratio calculated in the numerical solution, the relationship

$$f(D) = 1-0.428481\times10^{-5}D^2+0.101103\times10^{-7}D^3-0.711096\times10^{-11}D^4 \qquad (7)$$

has been found, which covers D in the range (0, 605.72) to better than $\pm$ 1.3 per cent.

2. COMPARISON WITH EXPERIMENT

White measured the variation with k of the ratio of γ_c to γ_s, the resistance coefficients in the curved and straight pipes for the same flux Q_s, and found that when the flow is laminar, his experimental results could be represented by the empirical formula

$$\frac{\gamma_s}{\gamma_c} = 1 - \left[1 - \left(\frac{11.6}{k}\right)^x\right]^{\frac{1}{x}} \qquad (8)$$

where x = 0.45, the formula being valid for $11.6 < k < 3000$. A plot of $\log \gamma_c/\gamma_s$ against log k is given in figure 1, based on White and on Goldstein (1938).

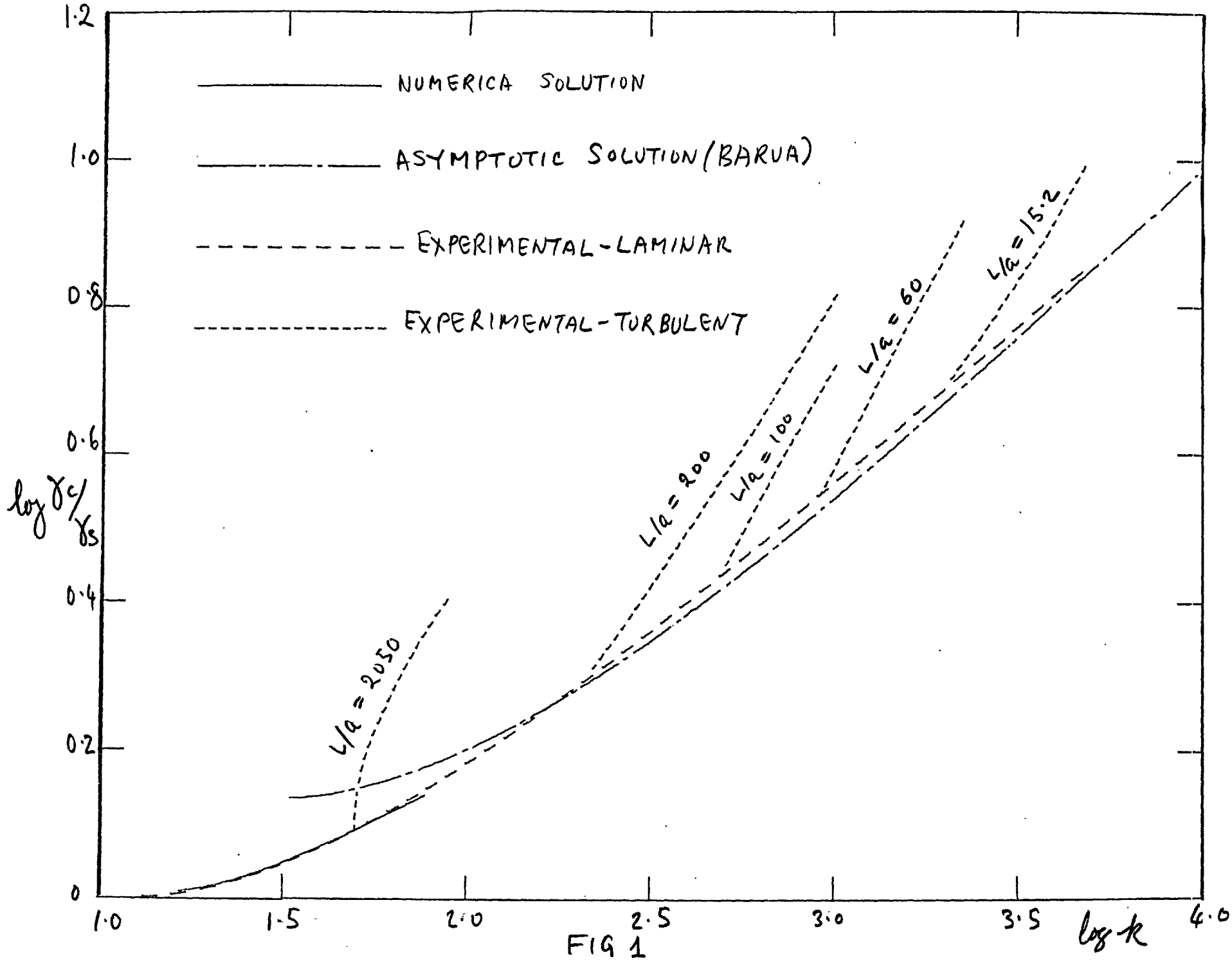
NUMERICA SOLUTION
ASYMPTOTIC SOLUTION (BARUA)
EXPERIMENTAL - LAMINAR
EXPERIMENTAL - TURBULENT
L/a = 2050
L/a = 200
L/a = 100
L/a = 60
L/a = 15.2
log γc/γs
log k
1.2
1.0
0.8
0.6
0.4
0.2
0
1.0
1.5
2.0
2.5
3.0
3.5
4.0

FIG 1

It can be shown that

$$\frac{\gamma_s}{\gamma_c} = \frac{Q_c}{Q_s} \qquad (9)$$

and a logarithmic plot of the reciprocal of the calculated flux ratio as a function of k for $16.60 < k < 77.05$ ($1.22 < \log k < 1.89$) is superimposed on the logarithmic plot of White's relationship in figure 1.

The agreement is close, as is to be expected from an exact solution of what are virtually the complete equations of motion. The only simplification of the Navier-Stokes equations is in taking the radius of curvature in the centrifugal body-force term to be constant over the cross-section of the pipe, and equal to L; for small a/L, the physical effects of this assumption should not be significant. In White's experiments, a/L was in the range (0.00049, 0.066).

3. RELATIONSHIP TO THE ASYMPTOTIC SOLUTIONS

The asymptotic solutions for large k developed by Barua and by Mori and Nakayama are based on two simplifying assumptions about the secondary-flow field. The first is that the viscous forces are of the same order as the inertia forces only in a thin boundary layer close to the wall of the tube. The second is that the motion outside the boundary

layer is confined to planes parallel to the plane of symmetry of the tube. Neither of these assumptions was based on any firm theoretical or experimental evidence. However, the exact field patterns produced by the numerical solution, especially those for D = 382.18, 481.14 and 605.72 establish the physical accuracy of this model, since they show both a central core in which the secondary flow streamlines are parallel to the plane of symmetry, and a boundary layer.

For the resistance ratio, Barua's solution provides the relationship

$$\frac{\gamma_c}{\gamma_s} = \frac{(1.22)^3}{4k}\left[1.81+\left\{(1.81)^2+\frac{k}{\sqrt{6}}\right\}^{\frac{1}{2}}\right]^3 \qquad (10)$$

A logarithmic plot of this is superimposed on White's empirical curve in figure 1, to give a quantitative indication of the range of validity of Barua's solution, and its relationship to the numerical solution, On the basis of its prediction of the resistance ratio, Barua's solution appears to be reasonably accurate for $k > 100$. The numerical solution thus bridges the gap between the perturbation and asymptotic solutions by providing a detailed picture of how the field patterns for the perturbation solution change progressively into those for the asymptotic solution with increasing k.

4. TRANSITION TO TURBULENCE

White found that for each of the three pipes tested in his experiments, there was a critical value of k below which the measured values of γ_c / γ_s lie on the common curve given by equation (8), but above which they leave the curve steeply, as shown in figure 1. The critical k depends on the curvature ratio a/L, and increases as a/L increases. White attributed this result to the fact that the turbulence at the inlet to the pipes no longer dies out above this critical k, and this conjecture was verified experimentally by Taylor (1929). The existence of the critical k has also been observed by Adler. White found that the onset of turbulence for each pipe occurred at

$$\gamma_c = \frac{-1}{L} \frac{\partial P}{\partial \theta} \rho \frac{a}{W_m^2} = 0.0090 \qquad (11)$$

where L θ is distance along the axis, and P the pressure; Adler's measurements are compatible with this (Goldstein).

The effect of increasing the curvature ratio for a tube is thus to increase the critical value R_{crit}, of the Reynolds number R (customarily taken to be $2W_m a/\nu$) below which turbulence is damped out after a certain length, but above which any turbulence persists. For straight pipes, R_{crit} is about 2000. A plot of R_{crit} versus a/L is shown in figure 2 based on Keulegan and Beij (1937) who analysed the results of White, Taylor and Adler.

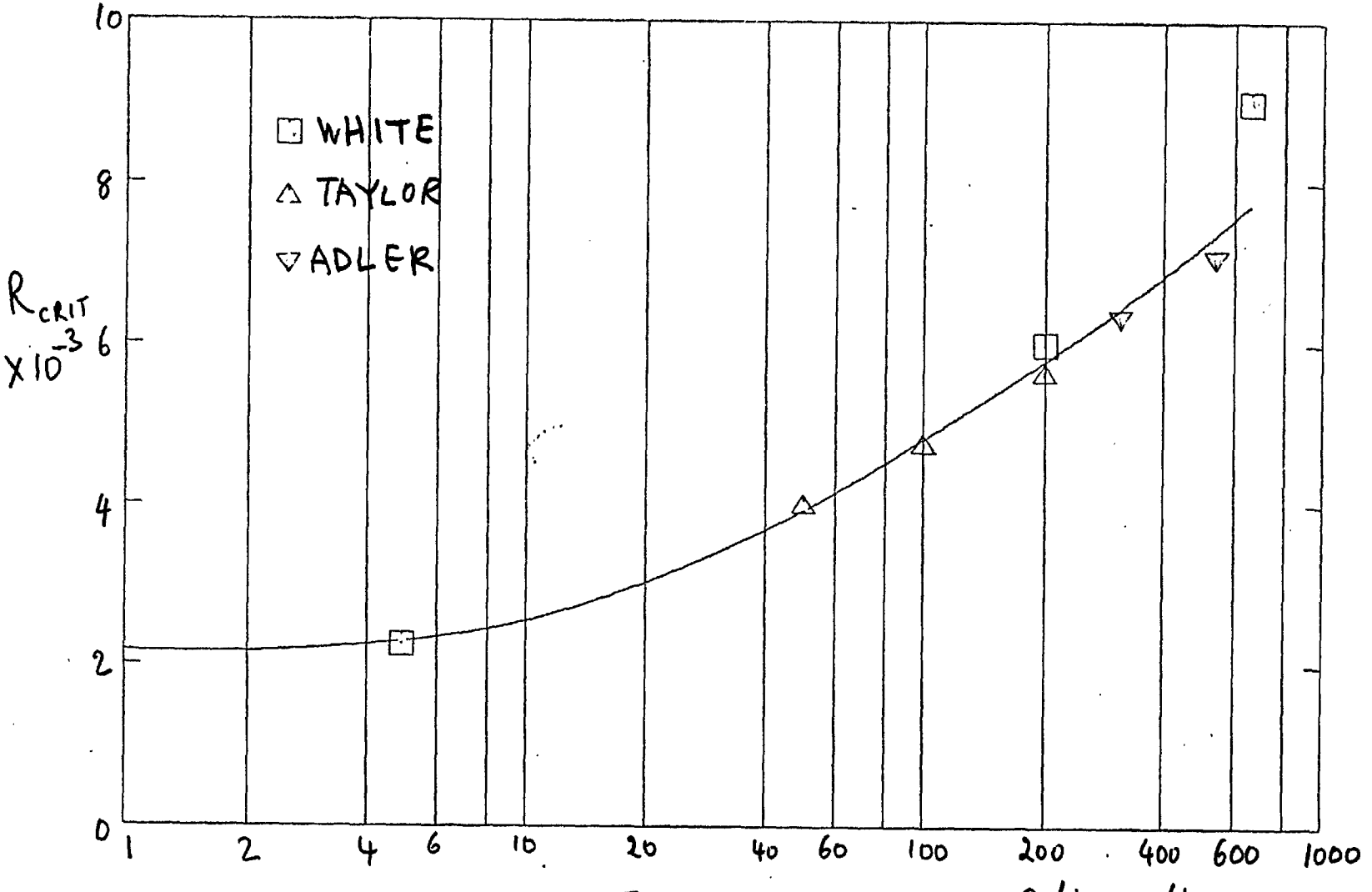
WHITE
TAYLOR
ADLER
R_{CRIT} X 10^{-3}
0
2
4
6
8
10
1
2
4
6
10
20
40
60
100
200
400
600
1000
a/L X 10^4

FIG 2

This well-established experimental fact has not so far been satisfactorily explained. Lighthill (1969) argues that an interpretation might reasonably be based on the boundary-layer model, now that its physical accuracy has been established by the numerical solution of the complete equations. For a curved tube, all the vorticity is confined within a boundary layer of thickness δ which is a small fraction of a, the tube radius, and δ/a decreases as a/L increases. Now the usual type of transition criterion depends on a Reynolds number based on boundary-layer thickness, and for a curved tube, might depend on some value of such a Reynolds number, say

$$R_c = \frac{2W_m \delta}{\nu} \qquad (12)$$

The corresponding critical Reynolds number based on the tube diameter would be

$$R_{crit} = \frac{R_c}{\delta/a} \qquad (13)$$

and would increase as a/L increases.

These arguments presuppose no net influence on stability from centrifugal effects, which are destabilizing nearer to the outside of the bend than the position of maximum axial velocity, but stabilizing nearer to the inside.

5. THE EFFECT OF SECONDARY FLOW ON THE DISPERSION OF INJECTED SOLUTE

The flow fields obtained in the iterative Fourier-series solution are now applied to study the dispersion of a substance introduced into the tube by analysing how the particles of the substance are variously convected, depending on the streamlines on which they have been deposited. Such an analysis based on a continuum model takes no account of the other dispersive factor, molecular diffusion, present in all real fluids. It will therefore be physically accurate only for fluids in which convection is the predominant agent.

In Poiseuille flow, convective dispersion is purely axial, and is brought about by the different axial velocities of the particles, depending on their radial distances from the axis. Any transverse diffusion is due to molecular diffusion. In flow through a curved tube, in which secondary flow causes convective radial dispersion, a measure of the relative importance of convection and diffusion for a particular fluid is given by the relative sizes of its kinematic viscosity ν and its molecular diffusivity K. One effect of radial diffusion of the molecules is to diffuse the axial momentum, since molecules from faster regions will move to slower regions and vice versa. The total diffusion of axial momentum is, however, much greater, being measured by the kinematic viscosity ν. Convection and diffusion are in balance for

the axial momentum. However, for liquids, ν and κ are respectively of order 10^{-2} and 10^{-5} $cm^2/sec.$, so that κ plays a role three orders of magnitude less than that of ν. Hence convection may be much more important than diffusion for transfer of an introduced substance. For gases, both are of order 10^{-1} cm^2/sec. The effects of diffusion, however, increase with time, the root mean square linear displacement in time t seconds being

$$\bar{x} = \sqrt{2\kappa t},$$

so that the results of this convective analysis would be valid for a tube of radius a only for a time $t \ll a^2/\kappa$ after injection.

The present analysis assumes that the injected particles are dynamically indistinguishable from the fluid particles, and is therefore valid only for a substance of the same density as the fluid.

The iterative solution provides sufficient information to enable the three-dimensional path and velocity of any particle of the fluid to be calculated, so in principle, a complete three-dimensional analysis of the convective diffusion of an injected substance of arbitrary initial distribution could be carried out. Such a complete physical picture would be difficult to interpret and present, so some simplifying assumptions and limitations must be introduced at the outset.

1) The non-dimensional time T taken for the particle to traverse its closed secondary-flow streamline. The secondary-flow streamline for a particle is sometimes described as the projection of its helical path on the cross-section; it can be thought of more accurately as the actual path of the particle in a cross-section which moves axially with the particle. Streamlines are defined by $\phi = \phi_c$ where ϕ is the secondary-flow stream function and ϕ_c is a constant.

2) The non-dimensional axial distance ℓ which the particle travels in time T.

3) The area A enclosed by its streamline.

The study of axial dispersion in a curved tube is complicated by the fact that a particle does not have a uniform axial velocity, since w may vary widely at different points of the secondary-flow streamline. This leads to the third simplification through the definition of a mean velocity for the particle

$$\bar{w} = \ell/T \qquad (15)$$

An analysis in terms of the statistical distribution of $\bar{w}$ will, of course, only give an accurate picture at a considerable distance from the site of the injection. This will be considered quantitatively later.

The area A enclosed by the streamline given by $\phi = \phi_c$ is used to derive the independent variable F, in terms of

which the statistical distributions of T, ℓ and $\bar{w}$ over the partcles of the injected substance are presented. F is a monotonic decreasing function of ϕ, and is defined by

$$F(\phi_c) = \frac{2A}{\pi} \tag{16}$$

so that $F(0) = 1$, and $F(\phi_{max}) = 0$, ϕ_{max} being the maximum value of ϕ. Let T_A and T_B, ℓ_A and ℓ_B and $\bar{w}_A$ and $\bar{w}_B$ be the times, lengths and velocities associated with the streamlines defined by $\phi = \phi_A$ and $\phi = \phi_B$, $\phi_A > \phi_B$, and $\Delta F = F(\phi_B) - F(\phi_A)$ Then the proportion of the total fluid in the upper half of the tube circulating between these streamlines is given by ΔF, and since T, ℓ and $\bar{w}$ are monotonic functions of ϕ, ΔF will give the proportion of the fluid in the upper half of the tube with time, length and velocity in the ranges (T_B, T_A), (ℓ_B, ℓ_A) and $(\bar{w}_A, \bar{w}_B)$. Since the flow fields are symmetrical about the central diameter, ΔF will give the fraction of the total fluid in the tube with the above distribution of physical properties, and the distribution over the injected substance.

The non-dimensional quantities T and ℓ are given by line integrals. A particle at any point on its secondary-flow streamline defined by $\phi = \phi_c$ will have a velocity along the streamline given by $\partial\phi/\partial n$, the derivative in the direction normal to the streamline at the point. If s is the distance along the streamline measured from some convenient point, the time dt to travel distance ds will be

$$dt = \frac{ds}{\frac{\partial \phi}{\partial n}} \tag{17}$$

and in time dt it will travel a distance wdt in the axial direction, w being the axial velocity at the point. The total time of circulation T of the particle around the streamline is then

$$T(\phi_c) = \oint \frac{ds}{\frac{\partial \phi}{\partial n}} \tag{18}$$

and the total distance ℓ travelled in the axial direction is

$$\ell(\phi_c) = \oint \frac{w\,ds}{\frac{\partial \phi}{\partial n}} \tag{19}$$

both line integrals being taken around the closed streamline $\phi = \phi_c$.

The integral for T in (18) can be transformed into a derivative which provides an alternative calculation of T. If A and A + Δ A are the areas enclosed by the streamlines $\phi = \phi_c$ and $\phi = \phi_c + \Delta\phi$ (ϕ is taken as positive so that $\Delta A < 0$ if $\Delta\phi > 0$), then

$$\oint \frac{ds}{\frac{\partial \phi}{\partial n}} = \lim_{\Delta\phi \to 0} \oint \frac{ds}{\frac{\Delta \phi}{\Delta n}}$$

$$= \lim_{\Delta\phi \to 0} \frac{1}{\Delta\phi} \oint \Delta n\, ds = -\lim_{\Delta\phi \to 0} \frac{\Delta A}{\Delta\phi}$$

or

$$T = -\frac{dA}{d\phi} \tag{20}$$

since Δn at any point is the distance between the curves along their limiting common normal. This expression was used as an independent check on the calculations of T, being particularly convenient as A had to be calculated to get F.

6. NUMERICAL METHODS FOR CALCULATING T, l AND A

Each integrand in (18) and (19) can be obtained in discrete one-dimensional form, as a periodic function defined at unequal intervals of the independent variable s, and the integrals can then be evaluated by any suitable combination of interpolation and integration. The coordinates of a sequence of points on a streamline defined by $\phi = \phi_c$ can be calculated, together with the values of the integrands at these points. The directions of the tangents to the streamline at the points are obtained in the process of calculating $\partial\phi / \partial n$ at the points, and these directions and coordinates are used to construct the streamline, to give the arc lengths between adjacent points of definition of the integrands.

$$\text{Now } \frac{\partial \phi}{\partial n} = |\nabla \phi| = \left\{ \left(\frac{\partial \phi}{\partial r}\right)^2 + \left(\frac{1}{r}\frac{\partial \phi}{\partial \alpha}\right)^2 \right\}^{\frac{1}{2}} \qquad (21)$$

and $\partial\phi/\partial r$ and $1/r(\partial\phi/\partial\alpha)$ are given as Fourier series whose coefficients are directly calculated in the process of the iterative solution. The iterative solution gives w, ϕ, $\partial\phi/\partial r$

and $1/r(\partial\phi/\partial r)$ at the eleven points r = 0(0.1)1 along any radius at an angle α. Cubic spline interpolation (Greville 1967) was used to give a continuous representation of the four quantities for all r in the range (0, 1).

For each value of D, the quantities were evaluated on radii at an angular spacing of 2° from $\alpha = 2°$ to $\alpha = 178°$. The coordinates of the intersections of these radii with the streamline $\phi = \phi_c$ were found by direct interpolation from the approximations for ϕ along the radii, and the values of w, $\partial\phi/\partial r$ and $1/r(\partial\phi/\partial\alpha)$ at these points of intersection from the corresponding approximations.

In addition to defining $\partial\phi/\partial n$ at the point (r, α) on the streamline, $\partial\phi/\partial r$ and $1/r(\partial\phi/\partial\alpha)$ being $-(a/\nu)V$ and $(a/\nu)U$, where U and V are the radial and transverse components of velocity, also determine the slope of the streamline at the point. In Cartesian coordinates, which are used for constructing the streamline, the relationship

$$\frac{dx}{\frac{1}{r}\frac{\partial\phi}{\partial\alpha}\cos\alpha + \frac{\partial\phi}{\partial r}\sin\alpha} = \frac{dy}{\frac{1}{r}\frac{\partial\phi}{\partial\alpha}\sin\alpha - \frac{\partial\phi}{\partial r}\cos\alpha} \qquad (22)$$

holds. From (22), the sines and cosines of the slopes were calculated separately.

The algorithm for constructing the streamlines was developed to treat the x- and y-coordinates symmetrically (and hence independently of axis orientation) and to

incorporate the known values of the slopes. The complete streamline is represented by a sequence of separate arcs joining adjacent points, these arcs having the calculated slopes at their end points, thereby giving the complete curve tangential continuity. Let P_q denote the point (x_q, y_q) on the streamline, and θ_q the angle which the tangent at P_q makes with the x-axis. The x- and y-coordinates of the arc joining P_q to the adjacent point P_{q+1} are defined separately as cubics in a parameter t, which varies from t = 0 at P_q, to t = T_q at P_{q+1}. The cubics arise from integrating separate quadratic expressions for dx/dt and dy/dt constructed to give them the values $\cos\theta_q$, $\sin\theta_q$ and $\cos\theta_{q+1}$ and $\sin\theta_{q+1}$ at P_q and P_{q+1}, and with one parameter to satisfy the end conditions on integration. The expressions for the derivatives are:-

$$\frac{dx}{dt} = \cos\theta_q + (\cos\theta_{q+1} - \cos\theta_q)t/T_q + C_q t(T_q - t)$$
$$\frac{dy}{dt} = \sin\theta_q + (\sin\theta_{q+1} - \sin\theta_q)t/T_q + D_q t(T_q - t) \qquad (23)$$

Taking x_q and y_q as the constants of integration, and the condition that $x = x_{q+1}$, $y = y_{q+1}$ at P_{q+1} determines C_q and D_q.

The curve generated will depend on the value of T_q, but for all T_q it will have the required value of dy/dx at P_q and P_{q+1} and also

$$\frac{ds}{dt} = \left\{\left(\frac{dx}{dt}\right)^2 + \left(\frac{dy}{dt}\right)^2\right\}^{\frac{1}{2}} \qquad (24)$$

will be unity at these points, s being the arc length measured

from P_q. The total arc length is then

$$S_q = \int_0^{T_q} \frac{ds}{dt}\, dt \qquad (25)$$

The optimum T_q is taken to be the one which minimises the departure of ds/dt from unity over the range $(0, T_q)$ on the least-squares criterion, the determining equation being

$$\frac{d}{dT_q} \int_0^{T_q} \left(\frac{ds}{dt} - 1\right)^2 dt = 0 \qquad (26)$$

Equation (26) would have to be solved by numerically minimizing the integral. This, however, is not necessary, since in the neighbourhood of the optimum T_q, the value of dS_q/dT_q is so small that an adequate approximation to the optimum T_q is obtained as a root of the quadratic equation in T_q which results from making $ds/dt = 1$ at $t = T_q/2$.

Equation (25) must be evaluated numerically, and as the integrand is knwon in the middle of the range and at both ends, an odd-order Lobatto quadrature formula (Krylov 1962) is the most efficient; the five-point formula (requiring two evaluations of ds/dt) is adequate.

The area enclosed by the streamline is obtained by calculating

$$A_q = \frac{1}{2} \int_0^{T_q} \left(x \frac{dy}{dt} - y \frac{dx}{dt}\right) dt \qquad (27)$$

for each arc, using equations (23) and their integrated forms, and summing over all the arcs.

The adequacy of equations (23) and (27) in the present calculations was checked by repeating selected calculations with radii spaced at 3° and 5° apart. The results were sensibly the same as those for the 2° spacing. The alternative expression for T, namely $-d\Lambda/d\phi$ was calculated by numerical differentiation as a further check on the calculation of (18), and corresponding values agreed closely.

One refinement was introduced to cope with the indeterminacy of $w/(\partial\phi/\partial n)$ on the boundary $r = 1$. This indeterminacy can be resolved by applying L'Hospital's rule to the square of the integrand giving

$$\lim_{r\to 1} \frac{w}{\frac{\partial\phi}{\partial n}} = \left\{ \lim_{r\to 1} \frac{w^2}{\left(\frac{\partial\phi}{\partial r}\right)^2 + \left(\frac{1}{r}\frac{\partial\phi}{\partial\alpha}\right)^2} \right\}^{\frac{1}{2}}$$

$$= \frac{\frac{\partial w}{\partial r}(1)}{\zeta(1)}$$

where $\zeta(1)$ is the vorticity on the boundary.

On any radius which intersected a streamline near the boundary $r = 1$, the integrand in (19) was obtained by cubic interpolation from the values of the ratio at the adjacent points $r = 0.7$, 0.8, 0.9 and the value at $r = 1$ calculated directly from (28) instead of by three separate spline interpolations for w, $\partial\phi/\partial r$ and $1/r(\partial\phi/\partial\alpha)$.

In the early stages of the work, the integrals were calculated by representing the integrand between the points

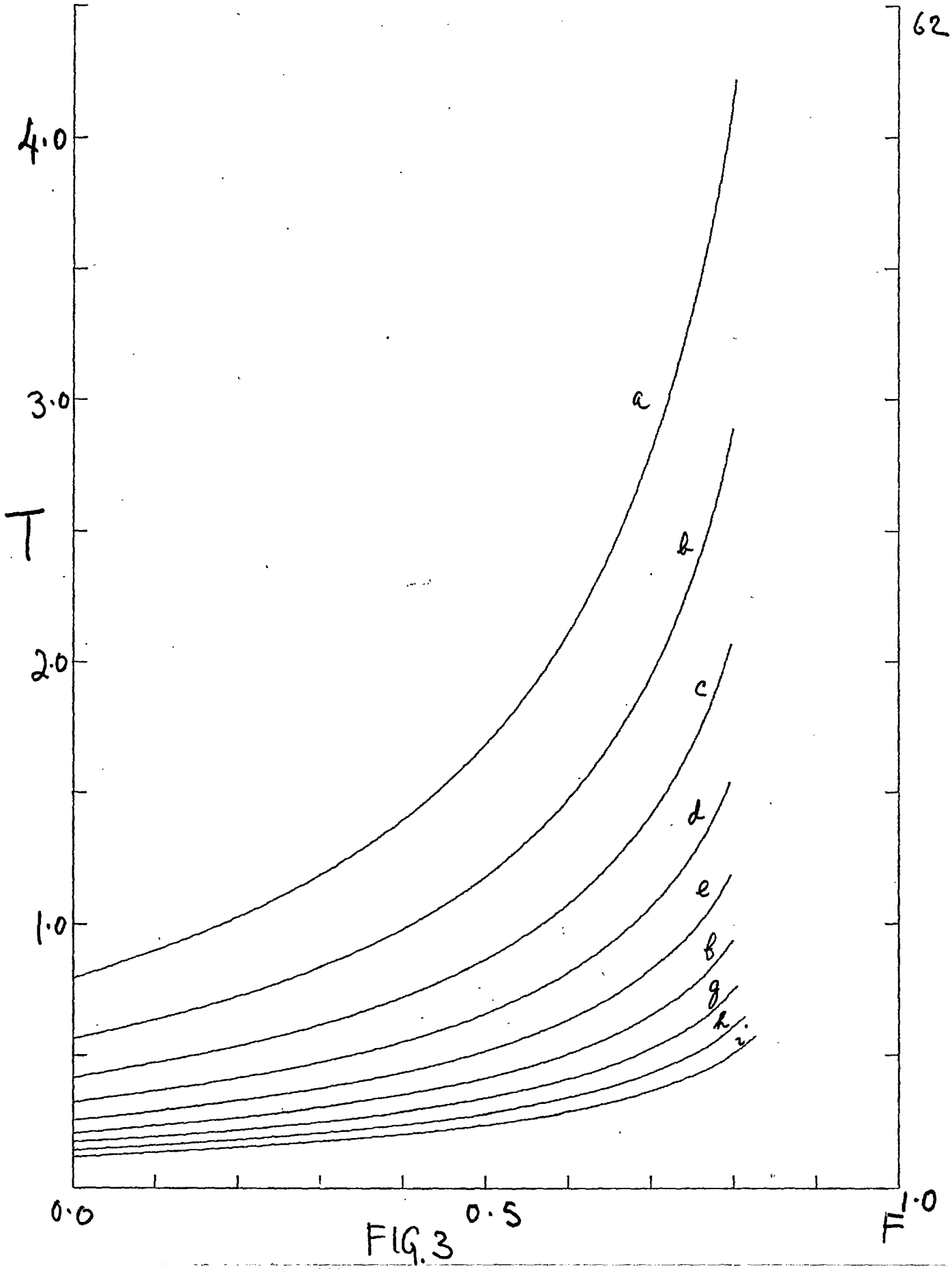

FIG. 3

of definition by cubic Lagrangian interpolation using the values at the end points of the interval and the adjacent points on each side and integrating this. This was later replaced by cubic spline integration (Greville). Corresponding results from the two algorithms did not differ significantly.

7. PRESENTATION OF THE RESULTS

Plots of T and ℓ calculated from equations (18) and (19) against F are given in figures 3 and 4. At F = 1, corresponding to $\phi = 0$, the limiting streamline is the central diameter and the semi-circular wall of the tube, and $-dF/d\phi$ is infinite. The numerical techniques for the line integrals are inadequate close to this singularity, and values of the integrals above F = 0.8 have not been calculated. This corresponds to a ϕ_c about 0.9 times the maximum value of ϕ on a radius at an angle of 2° to the diameter, so that the streamline passes very close to the central diameter. For all D, the curves for T and ℓ are asymptotic to F = 1. Also, close to ϕ_{max} (F = 0), the numerical techniques again become unreliable, since $\partial\phi/\partial n$ approaches zero, making the integrands approach infinity, as the path lengths tend to zero. Here, however, extrapolation from adjacent reliable values is legitimate.

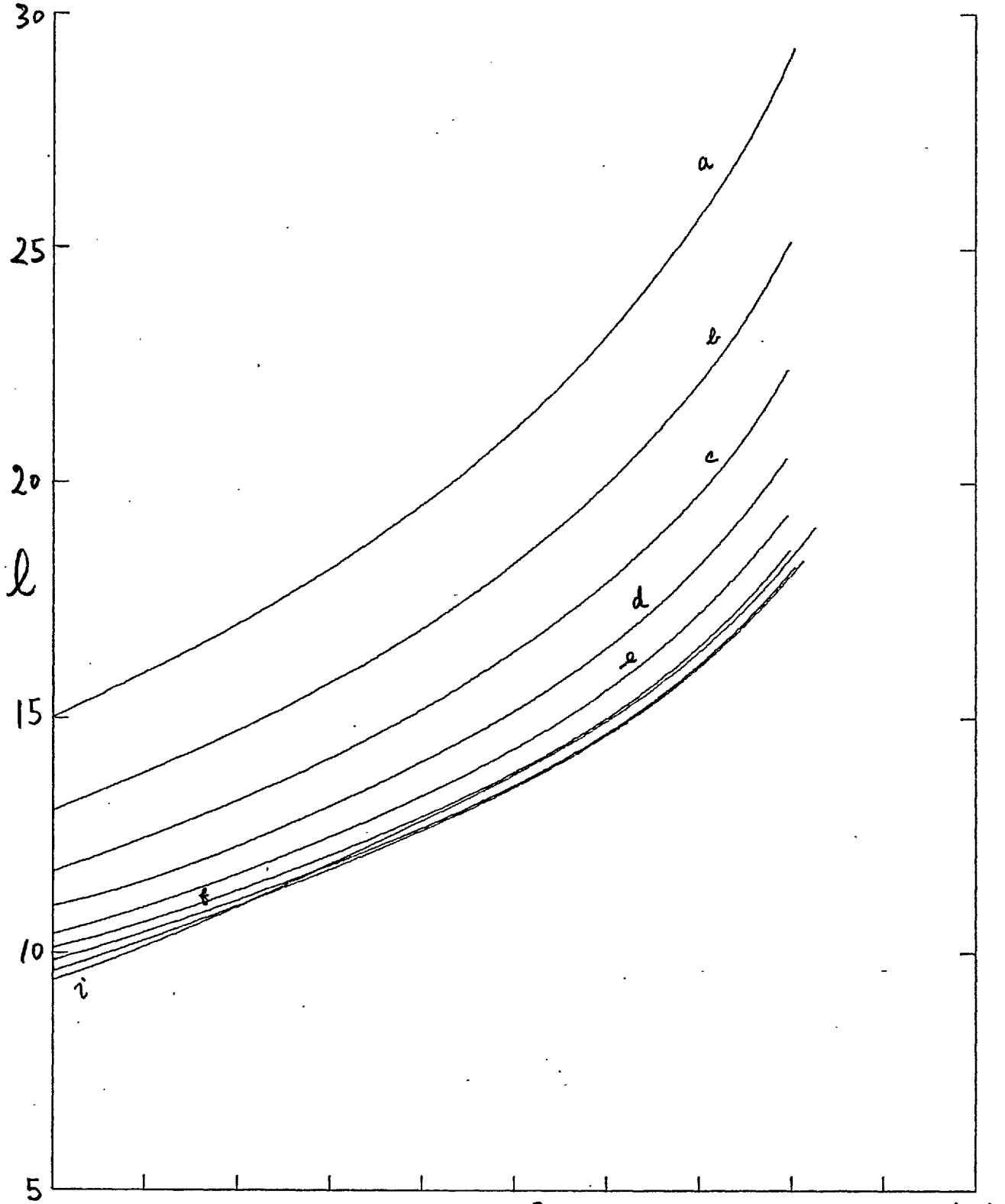

FIG. 4

Figure 4 shows that the curves of ℓ for the larger values of D tend to bunch. Such an effect is implicit in the asymptotic solution, and its occurrence in these calculations is a further indication that the upper end of the numerical solution approaches the lower end of the asymptotic. Let ℓ_m be a dimensionless "median" length such that half the fluid has $\ell > \ell_m$, and half $\ell < \ell_m$; ℓ_m is the axial distance travelled by a particle on the streamline which encloses an area of $\pi/4$.

The plot of ℓ_m against k in figure 5 is seen to be consistent with the idea that ℓ_m is asymptotic to about 310 k^{-1} for small k and to a constant value of about 14 for large k. These non-dimensional values have to be multiplied by $\sqrt{(\frac{1}{2}aL)}$ to convert them to dimensional values. In dimensional terms, ℓ_m is about $110\nu L/aW_m$ for small k and about $10\sqrt{(aL)}$ for large k.

The types of proportionality involved here can be understood from considerations of force balance as follows. For small k, centrifugal forces of order W_m^2/L per unit mass must be balanced by viscous forces resisting the secondary flow. If a maximum secondary-flow velocity in dimensional terms is V_m, this suggests that W_m^2/L and V_m/a^2 are proportional, so that V_m is proportional to $a^2W_m^2/L$. But from the definition (19) of ℓ, ℓ_m may be expected to be proportional to $W_m a/V_m$, and therefore to $\nu L/aW_m$ in this range of k. For large k,

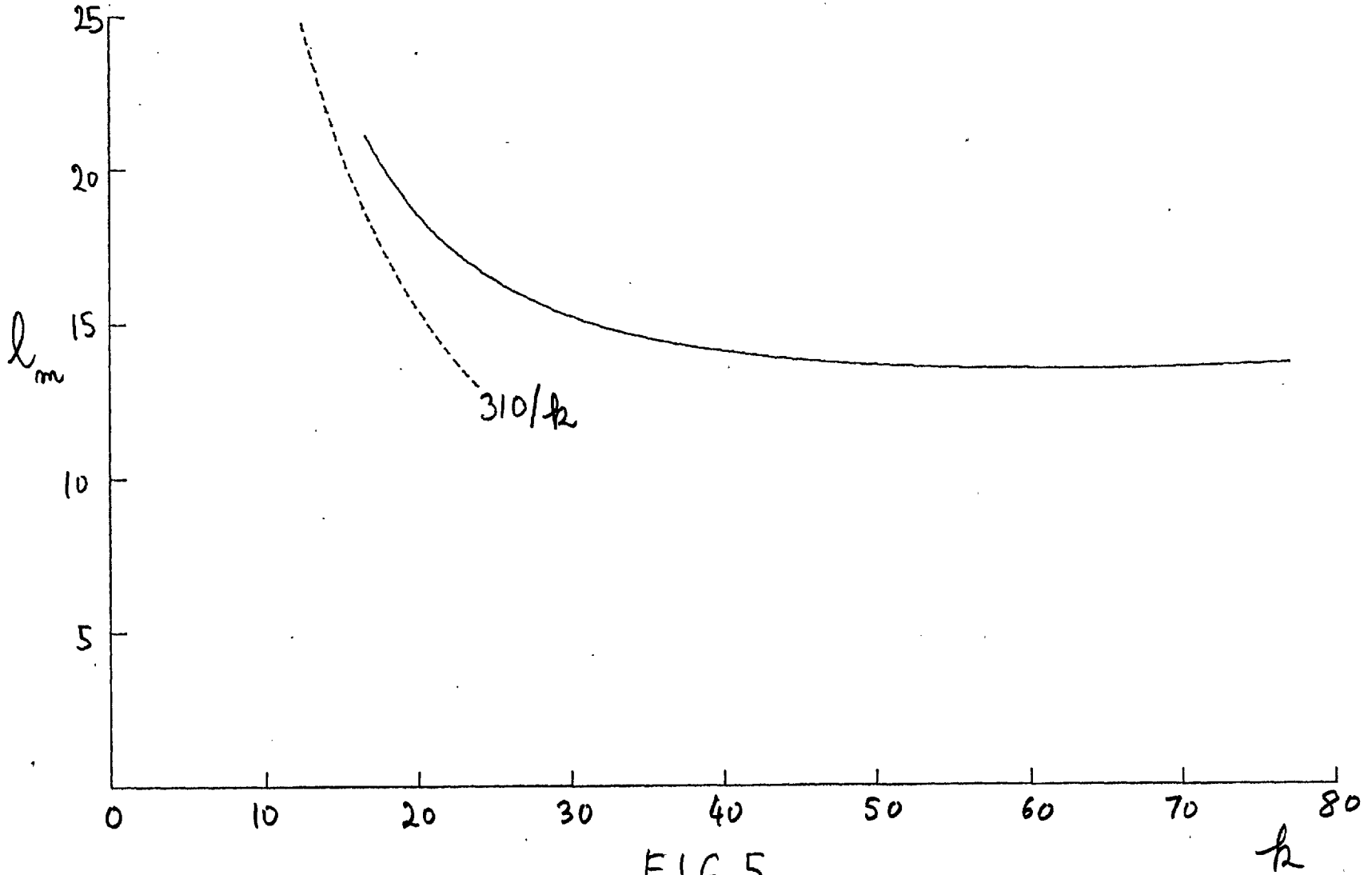

FIG 5

however, the centrifugal forces of order W_m^2/L must primarily be balanced by the inertial forces in the secondary flow, and these are of order V_m^2/a, suggesting that V_m is proportional to $W_m\sqrt{(a/L)}$ and so that ℓ_m is proportional to $\sqrt{(aL)}$. These arguments, on the other hand, give merely orders of magnitude, and the important conclusion from the computations is that for large k the typical distance ℓ_m in which a spiral streamline turns around once is actually as great as $10\sqrt{(aL)}$.

A plot of $\bar{W}/\bar{W}_{max}$ against F is given in figure 6, $\bar{W}_{max}$ being the maximum value of $\bar{W}$, which occurs at F = 0. This form was chosen to display the departure of the distribution of velocities from that for Poiseuille flow, in which since Δ F is proportional to Δ W, a plot of W/W_{max} against F would be the straight line joining (0,1) to (1,0).

Since particles at the wall of the tube have zero velocity, $\bar{W}$ = 0 at F = 1. No useful expression was found for the form of ℓ/T in the neighbourhood of F = 1. The curves were extended beyond F = 0.8 by cubic spline interpolation as far as F = 0.95, since any error in the shape of the extended curve must be small and physically unimportant in this region of low $\bar{W}$. The extensions are shown in dashed lines in figure 6. The values of $\bar{W}_{max}$ are given in table 1.

Because of secondary flow, particles close to the centre of the tube, and therefore in a region of high axial velocity are periodically carried into regions close to the wall of the

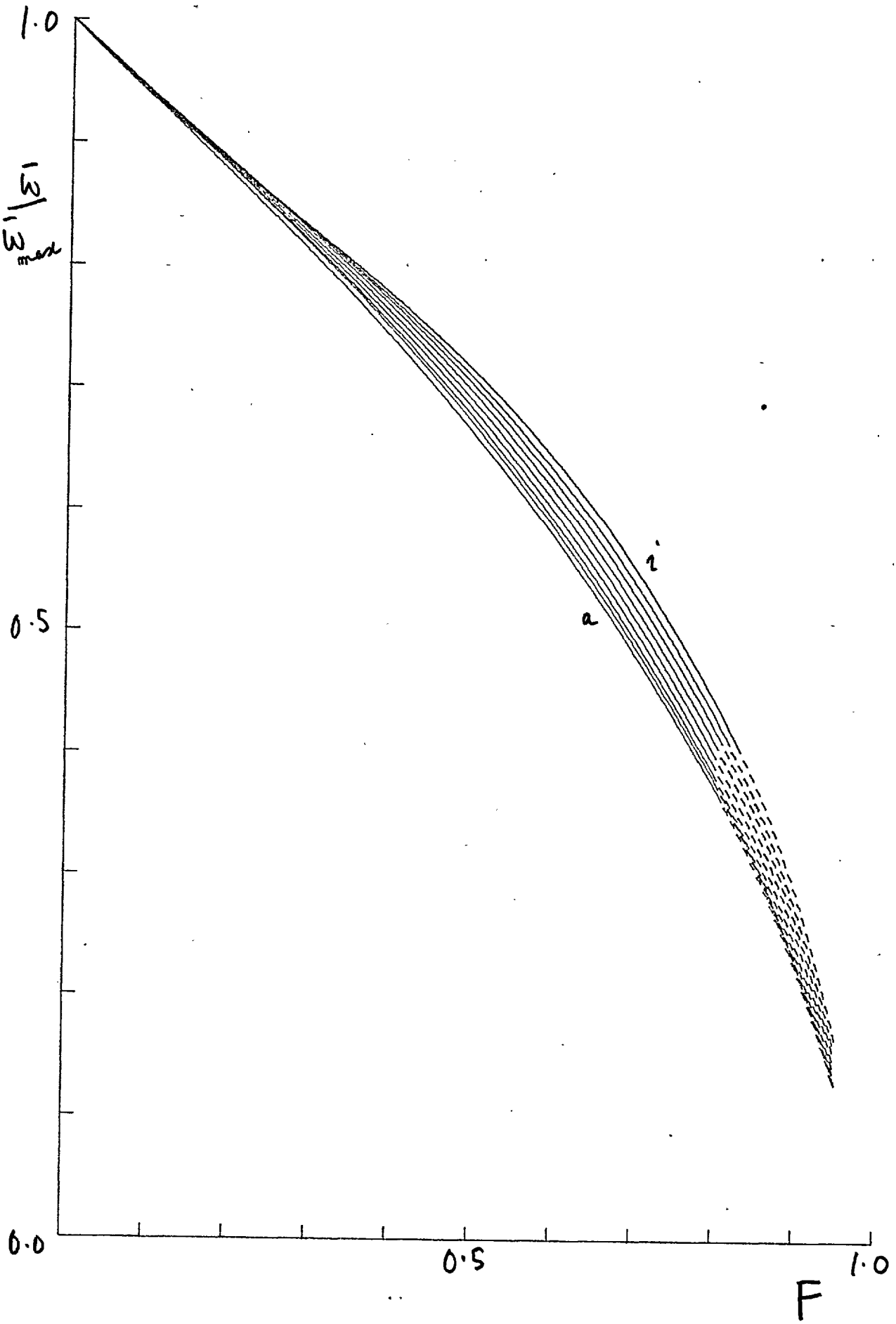
1·0
$\frac{\bar{w}}{\bar{w}_{max}}$
0·5
0·0
a
i
0·5
1·0
F

tube, of low axial velocity, and back again to the centre thereby narrowing the spread of mean velocity over the particles. This effect is seen in figure 6, where the departure of the distribution from that for Poiseuille flow is progressively, with increasing D, in the direction of the limiting rectangular distribution for all the particles having the same velocity.

As mentioned earlier, this periodic variation in the axial velocity means that the curves in figure 6 cannot be used to get a meaningful picture of dispersion close to the point of injection. For a particle injected at time t = 0, the ratio $\int_0^t w\,dt/\bar{w}t$ will oscillate with period T about unity with an amplitude decreasing as $1/\bar{w}t$, as t increases. The distribution in figure 5 therefore is only applicable after a time, and a corresponding distance large enough to make the periodic departure of the ratio from unity negligible for the bulk of the particles; this means at distances $\gg l_m$ the median length or $10\sqrt{(aL)}$ in terms of true lengths.

Experimental measurements of dispersion of an injected substance in straight and curved tubes have been reported by Caro (1966). In these, a thin bolus of dye was injected uniformly over the cross-section of the tube, and at a fixed distance X downstream, the variation with time of the concentration of dye inside a short section of tube of length ΔX was recorded. It was shown that convective dispersion by

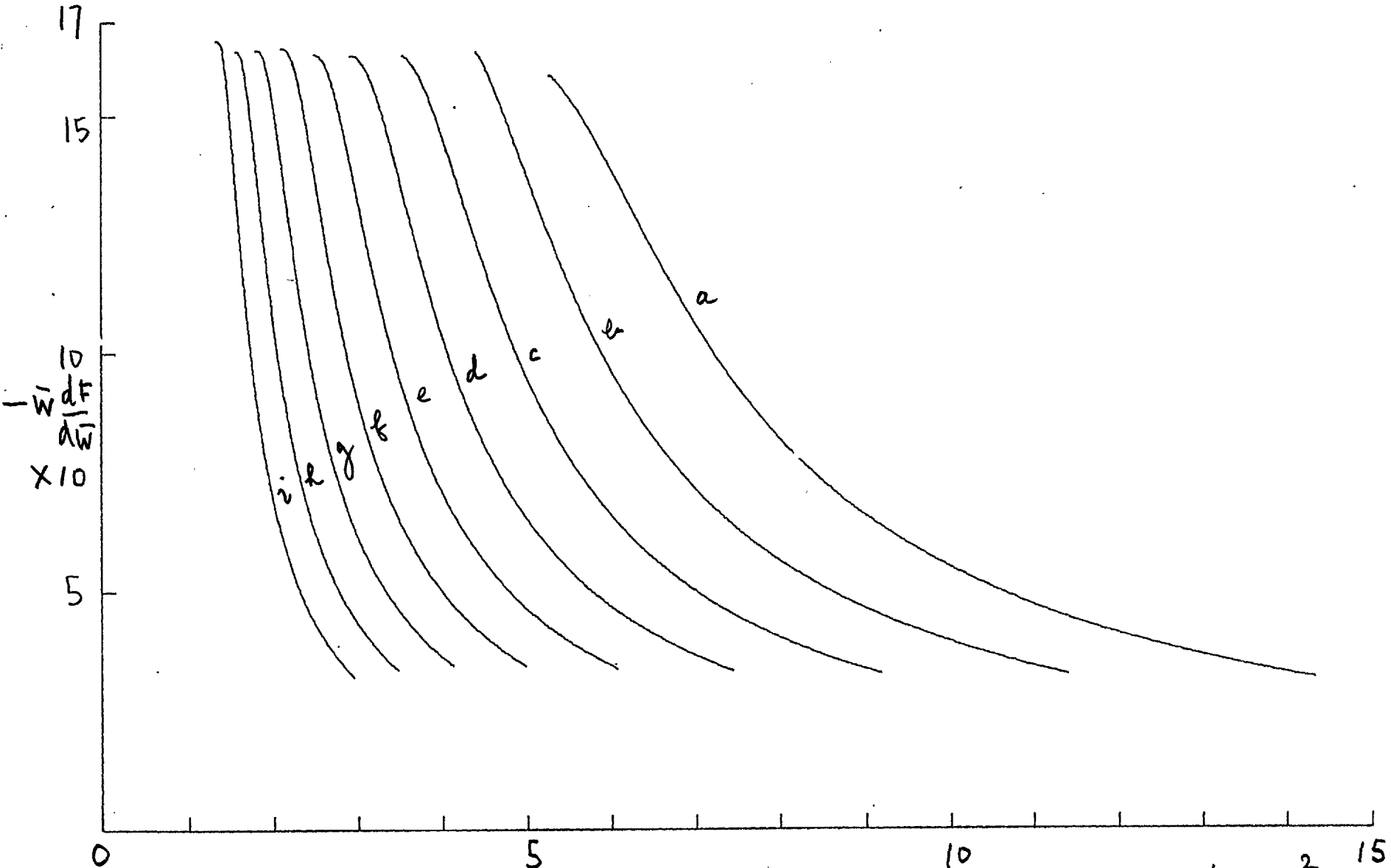
17
15
10
5
$-\bar{w}\frac{dF}{d\bar{w}}$
$\times 10$
a
b
c
d
e
f
g
h
i
0
5
10
15
$1/\bar{w} \times 10^2$

FIG. 7

Poiseuille flow would produce indicator concentration-time curves which are hyperbolic and this was borne out experimentally. It was also verified that the effect of tube curvature is to make the distribution of velocity over the injected particles more uniform, so that the bulk of the injected dye passes more quickly through the monitored region.

The present calculated values for $\bar{w}$ can be used to predict how the shapes of the indicator concentration-time curves vary with D for curved tubes. At time $t > (X + \Delta X)/\bar{w}_{max}$ after injection, the proportion of the dye inside the disc of length ΔX, is ΔF, the proportion of the fluid with velocity between $\bar{w}$ and $\bar{w} + \Delta\bar{w}$, where

$$\bar{w} = X/t \text{ and } \Delta\bar{w} = \Delta X/t$$

Since ΔF and $\Delta\bar{w}$ are both taken as positive,

$$F = -\frac{dF}{d\bar{w}}\Delta\bar{w} = -\frac{\Delta X}{X}\bar{w}\frac{dF}{d\bar{w}} \qquad (29)$$

Also, $t = X/\bar{w}$. The shape of the indicator concentration-time curve will thus be given by a plot of $-\bar{w}\frac{dF}{d\bar{w}}$ versus $1/\bar{w}$. The set of plots is given in figure 7.

The curves are asymptotic to the line $-wdF/d\bar{w} = 0$. For these curves, the calculated values of w had to be smoothed, since in the region of $F = 0$, $d\bar{w}/dF$ is very small, and the value of $dF/d\bar{w}$ is correspondingly sensitive to computational "noise". Least-squares cubic approximation was adequate.

The effect of secondary flow in levelling out the velocity distribution with increasing D is again evident.

The original scaling of the simplified Navier-Stokes equations implies that the dimensionless T, and w have to be multiplied by a^2/ν , $\sqrt{aL/2}$ and $(\nu/a)\sqrt{L/2a}$ to convert them to true times, lengths and velocities.

The author acknowledges his indebtedness to Professor M.J. Lighthill, Sec. R.S., Royal Society Research Professor, Imperial College, for his continued creative interest in the problem.

REFERENCES

Adler, M. 1934 Zeitschr. f. angew. Math. u. Mech. 14, 257

Barua, S.N. 1963 Quart. Journ. Mech. and Applied Math. 16, 61

Caro, C.G. 1966 J. Physiol. 185, 501

Dean, W.R. 1927 Phil. Mag. 4, 208

Dean, W.R. 1928 Phil. Mag. 5, 673

Goldstein, S. 1938 Modern Developments in Fluid Dynamics, Vol. 1 New York: Dover

Greville, T.N.E. 1967 Mathematical Methods for Digital Computers, Vol. II. Edited by Ralston & Wilf, p. 156, New York: Wiley

Keulegan, E.H. & Beij, K.H. 1937 Journ. Res. Nat. Bur. Stand. 18, 89

Krylov. V.I. 1962 Approximate Calculation of Integrals p. 172 New York: The Macmillan Co.

Lighthill, M.J. 1969 in Osborne Reynolds Centenary Volume Manchester. The University Press (to be published)

McConalogue, D.J. & Srivastava, R.S. 1968 Proc. Roy. Soc. A 307, 37

Mori, Y & Nakayama, W. 1965 Int. J. Heat Mass Transfer 8, 67

Taylor, G.I. 1929 Proc. Roy. Soc. A 124, 243

White, G.M. 1929 Proc. Roy. Soc. A 123, 645

APPENDICES

APPENDIX A

CALCULATION OF ARC LENGTHS AND AREAS

Integration of equations (23) of Chapter III and application of the conditions at $t = 0$ and $t = T_q$ gives

$$C_q = \frac{6}{T_q^3}\left[\Delta x_q - \frac{T_q}{2}(\cos\theta_q + \cos\theta_{q+1})\right]$$

and (1)

$$D_q = \frac{6}{T_q^3}\left[\Delta y_q - \frac{T_q}{2}(\sin\theta_q + \sin\theta_{q+1})\right]$$

where $\Delta x_q = x_{q+1} - x_q$ and $\Delta y_q = y_{q+1} - y_q$

The criterion for the optimum T_q given in equation (26) of Chapter III is based on heuristic considerations, rather than on any rigorous variational considerations. In testing the algorithm on known curves, it was found that the change in curvature across the points was minimised when S_q and T_q were equal for each arc. When this occurred, the equation $ds/dt - 1 = 0$ had a root somewhere in the open range $[0, T_{opt}]$ where T_{opt} is the value of T_q satisfying equation (26). Such a root was found to occur only for T_q lying in the narrow range $(T_{opt} - \epsilon, T_{opt} + \eta)$, $\epsilon + \eta \ll T_{opt}$; for $T_q > T_{opt} + \eta$, $ds/dt \geq 1$, for $T_q < T_{opt} - \epsilon$, $ds/dt \leq 1$ everywhere. A sufficiently good approximation to T_{opt} can thus be found by imposing the condition that $(ds/dt)^2$ should be unity at $t = T_q/2$. This condition gives rise to a quadratic

equation in T_q which can be written in the standard form

$$aT_q^2 + bT_q + c = 0$$

where

$$a = 7 - \sin\theta_q \sin\theta_{q+1} - \cos\theta_q \cos\theta_{q+1}$$

$$b = 6\left[\Delta x_q(\cos\theta_q + \cos\theta_{q+1}) + \Delta y_q(\sin\theta_q + \sin\theta_{q+1})\right]$$

and $$c = -18(\Delta x_q^2 + \Delta y_q^2)$$

The relevant root corresponds to the positive value of the discriminant.

The computer subroutine was applied to a number of curves including the set of points on the ellipse given parametrically by

$$x = 3 + \sqrt{2}\cos\theta$$
$$y = 2 + (1/\sqrt{2})\sin\theta \qquad (3)$$

the slopes at the points being obtained from the analytic expression. For 36 points given by $\theta = 10^\circ\ (10^\circ)\ 360^\circ$, the area ($\pi$) was given to an accuracy of 0.0004 per cent, and the maximum error in the arc length was 0.004, and occurred for the arcs adjacent to the major axis.

It has been found that S_q and T_q differ by a very small fraction of one per cent (in the previous example, the maximum difference was 0.0017 per cent) so that T_q is an adequate approximation to the arc length and could be used, if only the line integrals are required.

This algorithm, combined with another to supply slopes where these are not given is the one used for passing a

smooth curve through a sequence of points in producing the figures for the present thesis.

APPENDIX B

CUBIC SPLINES FOR INTERPOLATION AND INTEGRATION

The particular form of spline used in the present work has a separate cubic between each nodes ; no cubic continues from one panel into the next. If P_k denotes the node given by (x_k, y_k), the second derivative is written as the linear Lagrangian

$$\frac{d^2y}{dx^2} = \frac{(x_{k+1} - x)}{\Delta x_k} C_k + \frac{(x - x_k)}{\Delta x_k} C_{k+1} \qquad (1)$$

where C_k and C_{k+1} are the second derivatives at P_k and P_{k+1}, as yet arbitrary, but giving second derivative continuity across the nodes. This is integrated twice, and the constants of integration chosen to make the curve pass through P_k and P_{k+1} . The condition for first derivative continuity across the nodes is imposed, and this gives rise to a set of linear simultaneous equations connecting C_{k-1}, C_k and C_{k+1} at the point P_k. This system of equations is known to be under-determined since at the end points P_1 and P_n, there are no C_o and C_{n+1} respectively. In the present work, this indeterminacy was resolved by giving the cubics for the end panels the appropriate slope where this was available as with w and ϕ where dw/dr and $d\phi/dr$ were given by the iterative process. Where the end slopes were not readily available, as with $\frac{1}{r}(\partial\phi/\partial z)$ and $\partial\phi/\partial r$, C_o was linearly extrapolated from C_1 and C_2, and C_{n+1} from C_{n-1} and C_{n-2}.

In the line integrals, of course, the periodicity of the function made the system determinate,

This is the only departure from the scheme set out by Greville referred to in Chapter III, who arbitrarily sets C_o and C_n both zero. The scheme given by Greville for the solution of the simultaneous equations by successive over-relaxation was used, and found to be completely satisfactory. This was used only for the line integrals. For the other approximations, the independent variable was given at eleven fixed points, so two 9x9 matrices had to be inverted at the outset, one for each method of coping with the indeterminacy.

SUBSIDIARY MATTER IN SUPPORT OF CANDIDATURE

Of the two enclosed papers, my contribution was in analysis and numerical analysis. I assess my contribution to "Anharmonic Model for the Thermal Conductivity of Liquids" at about 40 per cent, and to "Mutual Diffusion in Dense Supercritical Fluids" at 20 per cent. It was anticipated that this paper would ~~be~~ have been published in "Molecular Physics" before the submission of this thesis. As this has not occurred, a typescript has been inserted.

Offprinted from the *Transactions of The Faraday Society*,
No. 534, Vol. 63, Part 6, June, 1967

ANHARMONIC MODEL FOR THE THERMAL CONDUCTIVITY OF LIQUIDS

Anharmonic Model for the Thermal Conductivity of Liquids

BY A. F. COLLINGS, J. K. HORROCKS, D. J. MCCONALOGUE* AND E. MCLAUGHLIN

Dept. of Chemical Engineering, Imperial College, London, S.W.7

Received 23rd January, 1967

On the vibrational model of thermal conductivity energy is transferred down the temperature gradient by a vibrational transfer mechanism. Using the Lennard-Jones and Devonshire lattice model of the liquid, vibrational frequencies are calculated which take into account terms up to the fourth power of the displacement. Use of these anharmonic frequencies and the corresponding specific heat gives better agreement between calculated and experimental thermal conductivities than was obtained previously on the harmonic oscillator model.

In a previous paper [1] on the thermal conductivity of liquids it was shown that the diffusive displacement type contribution to heat conduction was negligible and the main contribution arising from vibrational motion was given by

$$\lambda \simeq \lambda_{\text{vib}} = \sqrt{2} v C_v / a, \tag{1}$$

where v is the vibrational frequency, a the nearest neighbour distance and C_v the lattice specific heat at constant volume per molecule. The model assumes a lattice structure for the liquid and omits contributions to conduction from the internal modes, as studies of the thermal conductivities of isotopic molcules [2] and the dimensionless ratio [3] of thermal conductivity to viscosity $m\lambda/k\eta$ suggest that rotational and internal vibrational modes do not participate in energy transport in the liqud state, at least for simple molecules. m is the mas of a molecule, and k is Boltzmann's constant. This contrasts with the situation in the gas phase where corrections such as the Eucken factor are applied to take into account the role of internal degrees of freedom.

In order to evaluate eqn. (1) a specific model of the liquid must be chosen. Previous cases studied are those which consider the liquid as a system of harmonic oscillators [1] or hard-sphere particles in a rectangular cell.[4] As neither of these models is completely realistic only moderate agreement between theory and experiment is obtained. We have extended this work to take account of anharmonic oscillators up to the fourth power of the displacement and also the limiting case of pure quartic oscillators.

ANHARMONIC AND QUARTIC FREQUENCIES

As for the harmonic oscillator model, evaluation of the frequencies and specific heats is done using the Lennard-Jones and Devonshire theory [5] of liquids. On this model the change in potential energy of a molecule, displaced from the centre of its cell a distance r, due to its neighbours at the centres of their cells, is given by $\psi(r) - \psi(0)$. This change is an angle-dependent quantity but in the theory is replaced by an

*Centre for Computing and Automation

average value determined by considering the z nearest neighbours, as smeared uniformly over a spherical surface of radius a. For a f.c.c. lattice, $a^3 = \sqrt{2}\, v$, where $v = V/N$ is the volume per molecule and z the co-ordination number is 12.

If the intermolecular pair potential is of the 12 : 6 form with ε the potential minimum and σ the molecular diameter, then the theory gives

$$\psi(r)-\psi(0) = z\varepsilon[v^{*4}L(y)-2v^{*2}M(y)] \tag{2}$$

where $v^* = v_0/v$ and $v_0 = \sigma^3$, $L(y)$ and $M(y)$ are functions of the square of the reduced distance $y = (r/a)^2$. When all the atoms are at the centres of their cells

$$\psi(0) = z\varepsilon[1{\cdot}01v^{*4}-2{\cdot}41v^{*2}]. \tag{3}$$

Eqn. (2) and (3) are those of Wentorf, Buehler, Hirschfelder and Curtiss [6] which modify the original Lennard-Jones and Devonshire expressions to take into account the effect of second and third nearest neighbours.

Expanding eqn. (2) for the potential well to terms of the fourth power in r yields on using the known expression for $L(y)$ and $M(y)$

$$\psi(r)-\psi(0) = \frac{z\varepsilon}{a^2}[L_1v^{*4}-M_1v^{*2}]r^2+\frac{z\varepsilon}{a^4}[L_2v^{*4}-M_2v^{*2}]r^4+\text{etc.} \tag{4}$$

where $L_1 = 22{\cdot}11, L_2 = 200{\cdot}6$, $M_1 = 10{\cdot}56$ and $M_2 = 28{\cdot}67$. Eqn. (4) is of the form

$$\psi(r)-\psi(0) = P_1r^2-P_2r^4, \tag{5}$$

and as the motion of the molecule oscillating in the potential well satisfies the energy balance equation for terms to the fourth power in r,

$$m\dot{r}^2/2 = \mathscr{E}-P_1r^2+P_2r^4, \tag{6}$$

where m is the molecular mass; this enables the frequency to be determined.

The period τ of execution of a complete vibration follows [7] from eqn. (6) as

$$\tau = 4\sqrt{\frac{m}{2}}\int_0^{r_1}\frac{\mathrm{d}r}{(\mathscr{E}-P_1r^2-P_2r^4)^{\frac{1}{2}}}, \tag{7}$$

where r_1 is the positive real root of $P_1r_1^2+P_2r_1^4 = \mathscr{E}$ as the points at which the potential energy $P_1r_1^2+P_2r_1^4$ equals the total energy $\mathscr{E}$ gives the limits of the displacement. $\mathscr{E}$ is assumed to remain constant throughout the vibration and the potential minimum is taken to be the zero of energy.

Eqn. (7) may be rewritten

$$\tau = 4\sqrt{\frac{m}{2}}\int_0^{r_1}\frac{\mathrm{d}r}{P_2^{\frac{1}{2}}(\mathscr{E}/P_2-P_1r^2/P_2-r^4)^{\frac{1}{2}}}. \tag{8}$$

and since P_2 and P_1 are positive, then factorized and expressed eventually as a complete elliptic integral of the first kind as

$$\tau = \frac{1}{(\mathbf{a}^2+\mathbf{b}^2)^{\frac{1}{2}}}\left\{4\left(\frac{m}{2P_2}\right)^{\frac{1}{2}}\right\}K(\mathscr{K}), \tag{9}$$

where

$$K(\mathscr{K}) = \int_0^{\pi/2}\frac{\mathrm{d}\theta}{(1-\mathscr{K}^2\sin^2\theta)^{\frac{1}{2}}}, \tag{10}$$

$$\mathscr{K} = \mathbf{b}/(\mathbf{a}^2+\mathbf{b}^2)^{\frac{1}{2}}, \tag{11}$$

and

$$\mathbf{a}^2 = \tfrac{1}{2}\left\{\frac{P_1}{P_2} + \left(\frac{P_1^2}{P_2^2} + 4\frac{\mathscr{E}}{P_2}\right)^{\frac{1}{2}}\right\}, \tag{12}$$

$$\mathbf{b}^2 = \tfrac{1}{2}\left\{-\frac{P_1}{P_2} + \left(\frac{P_1^2}{P_2^2} + 4\frac{\mathscr{E}}{P_2}\right)^{\frac{1}{2}}\right\}. \tag{13}$$

It follows, therefore, that the anharmonic frequency ν_A is

$$\nu_A = \frac{(P_1^2 + 4\mathscr{E}P_2)^{\frac{1}{4}}}{2\sqrt{2}m^{\frac{1}{2}}} \frac{1}{K\left[\frac{1}{\sqrt{2}}\left\{1 - \frac{P_1}{(P_1^2 + 4\mathscr{E}P_2)^{\frac{1}{2}}}\right\}^{\frac{1}{2}}\right]}. \tag{14}$$

Unlike the harmonic case ($P_2 = 0$) where the frequency becomes

$$\nu_H = P_1^{\frac{1}{2}}/2\sqrt{2}m^{\frac{1}{2}}K(0), \tag{15}$$

the frequency of the anharmonic oscillator depends on the energy $\mathscr{E}$. In the pure quartic case ($P_1 = 0$) the frequency ν_Q

$$\nu_Q = (4\mathscr{E}P_2)^{\frac{1}{4}}/2\sqrt{2}m^{\frac{1}{2}}K(1/\sqrt{2}), \tag{16}$$

also depends on $\mathscr{E}$ which is, however, independent of volume and given by $9kT/4$. (Although we use the terms harmonic and quartic oscillators, P_1 and P_2 and hence the restoring force constants are functions of volume).

THERMODYNAMIC PROPERTIES

In order to complete the evaluation of eqn. (1) expressions are required for some of the thermodynamic properties of the systems. The appropriate partition function to be evaluated is

$$z = \left(\frac{2\pi mkT}{h^2}\right)^{\frac{3}{2}} z_{\text{config}} \exp\left[\frac{-\psi(0)}{2kT}\right], \tag{17}$$

where

$$z_{\text{config}} = \int \exp -[\{\psi(r) - \psi(0)\}/kT]\mathrm{d}^3r, \tag{18}$$

which for the anharmonic oscillator becomes z^A_{config}.

$$z^A_{\text{config}} = 4\pi\left(\frac{kT}{P_1}\right)^{\frac{3}{2}} \int_0^\infty \xi^2 \exp(-\xi^2) \exp(-\Xi\xi^4)\, \mathrm{d}\xi,$$

$$= 4\pi(kT/P_1)^{\frac{3}{2}} f(\Xi), \tag{19}$$

on replacing $P_1 r^2/kT$ by ξ^2 and writing $\Xi = kTP_2/P_1^2$.

The upper limit of integration in eqn. (19) was taken as infinity rather than the cell boundary. This makes no substantial difference to the results and was done so that similar integrations in (20) and (23) were analytic. For the harmonic case only the first term of eqn. (5) is included, therefore

$$z^H_{\text{config}} = 4\pi(kT/P_1)^{\frac{3}{2}} \int_0^\infty \xi^2 \exp(-\xi^2)\, \mathrm{d}\xi. \tag{20}$$

The integral in eqn. (20) is $\pi^{\frac{1}{2}}/4$, hence the total partition function for the anharmonic oscillator can be expressed in terms of the harmonic as

$$z^A = z^H\, 4f(\Xi)/\pi^{\frac{1}{2}}. \tag{21}$$

Likewise, the partition function for the quartic oscillator z^Q in terms of the harmonic is

$$z^Q = z^H\, \Gamma(\tfrac{3}{4})/\pi^{\frac{1}{2}}\Xi^{\frac{1}{4}}, \tag{22}$$

as

$$z^Q_{\text{config}} = 2\pi(kT/P_2)^{\frac{1}{4}}\int_0^\infty \xi^{\frac{1}{2}} \exp(-\xi^2)\, d\xi, \tag{23}$$

where the integral is $\frac{1}{2}\Gamma(\frac{3}{4})$ and Γ is the gamma function.

The thermodynamic properties of systems of anharmonic and quartic oscillations can therefore be expressed in terms of the corresponding harmonic case using the standard formulae connecting the partition function and the thermodynamic properties. The results necessary for the present work are

$$\left(\frac{U}{kT}\right)^A = \left(\frac{U}{kT}\right)^H + \frac{T}{f(\Xi)}\left(\frac{\partial f(\Xi)}{\partial T}\right)_v = \left(\frac{U}{kT}\right)^H + \frac{d\ln f(\Xi)}{d\ln \Xi}, \tag{24}$$

$$\left(\frac{C_v}{k}\right)^A = \left(\frac{C_v}{k}\right)^H + \left[2\frac{d\ln f(\Xi)}{d\ln \Xi} + \Xi^2 \frac{d}{d\Xi}\left\{\frac{1}{f(\Xi)}\frac{df(\Xi)}{d\Xi}\right\}\right], \tag{25}$$

where U and C_v are the internal energy and specific heat at constant volume per molecule respectively. Corresponding results for quartic and harmonic oscillators are well known.

NUMERICAL WORK

The integrals to be evaluated to determine the thermodynamic properties are of the form

$$I_n(\Xi) = \int_0^\infty \xi^n \exp(-\xi^2)\exp(-\Xi\xi^4)\, d\xi, \tag{26}$$

therefore $f(\Xi) = I_2(\Xi)$; $f'(\Xi) = -I_6(\Xi)$ and $f''(\Xi) = I_{10}(\Xi)$. These integrals cannot be evaluated analytically and numerical integration is necessary. The integrands being even functions of ξ about the origin have their odd-order derivatives zero at this end of the range of integration, and away from the origin all their derivatives go rapidly to zero with increasing ξ. The trapezoidal rule applied to such integrals gives a high order of accuracy as suggested by the Euler-Maclarin sum formulae.[8, 9] Sufficient accuracy was obtained with a step length of 0·1 applied to a region of ξ near the origin.

With the values of these integrals, $(U_{\text{config}}/kT)^A$ and $(C_{v\ \text{config}}/k)^A$ were generated as a function of $T^* = kT/\varepsilon$ and $v^* = v_0/v$ as

$$\Xi = \frac{T^*}{12v^{*2}}\frac{[L_2 v^{*2} - M_2]}{[L_1 v^{*2} - M_1]^2} \tag{27}$$

is a function of T^* and v^* only. Once $(U_{\text{config}}/kT)^A$ is known it is then possible to calculate v_A as

$$\frac{\mathscr{E}}{kT} = \left(\frac{U}{kT}\right)^A - \frac{\psi_0}{2kT} = 3 + \frac{d\ln f(\Xi)}{d\ln \Xi}. \tag{28}$$

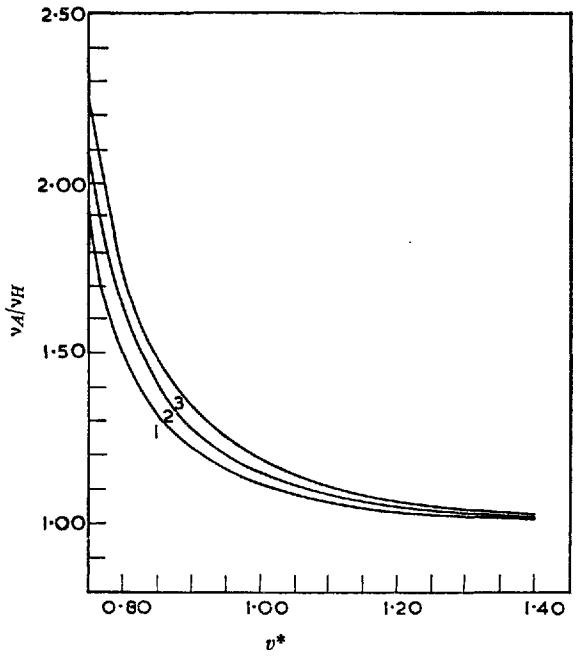

FIG. 1.—Anharmonic/harmonic frequency ratio as a function of v^*. Curve 1, $T^* = 0{\cdot}6$; curve 2, $T^* = 0{\cdot}9$; curve 3, $T^* = 1{\cdot}2$.

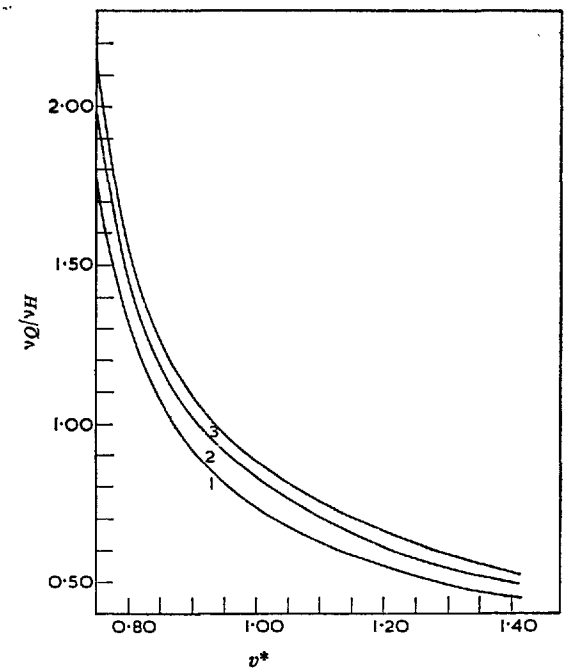

FIG. 2.—Quartic/harmonic frequency ratio as a function of v^*. Curve 1, $T^* = 0{\cdot}6$; curve 2, $T^* = 0{\cdot}9$; curve 3, $T^* = 1{\cdot}2$.

This was done as the ratio in the form

$$\frac{\nu_A}{\nu_H} = \frac{\pi}{2}\frac{(1-2\mathscr{K}^2)^{-\frac{1}{2}}}{K(\mathscr{K})} \tag{29}$$

where

$$\mathscr{K} = \frac{1}{\sqrt{2}}\left\{1-\frac{P_1}{(P_1^2+4\mathscr{E}P_2)^{\frac{1}{2}}}\right\}^{\frac{1}{2}},$$

$\mathscr{E}^* = \mathscr{E}/kT$ and $(1-2\mathscr{K}^2)^2 = (1+4\mathscr{E}^*\Xi)^{-1}$.

The tables obtained have not been included but cover a range of $T^* = 0{\cdot}6 \times 0{\cdot}05$ to 1·2 and $v^* = 0{\cdot}75 \times 0{\cdot}05$ to $\sqrt{2}$. As the main interest in the present work lies in the frequencies, these are plotted in fig. 1 for three values of T^* over the range of v^*. As expected, the ratio falls rapidly as the density of packing tends towards the close-packed structure where the vibrations are essentially harmonic. The internal energy and specific heat likewise tend to the equipartition values at the high density end.

The ratio of the quartic to the harmonic frequency is obtained from eqn. (15) and (16) as

$$\nu_Q/\nu_H = (4\mathscr{E}P_2)^{\frac{1}{4}}K(0)/K(1\sqrt{2})P_1^{\frac{1}{2}} = 1{\cdot}46746\ \Xi^{\frac{1}{4}}. \tag{30}$$

Fig. 2 gives the ratio ν_Q/ν_H as a function of v^* for three values of T^*.

APPLICATION TO THERMAL CONDUCTIVITY

With the available values of specific heat and the anharmonic frequencies, eqn. (1) can be evaluated. This has been done for a series of simple liquids using previous values of ε/k, σ and the densities. References to the experimental results are those

TABLE 1.—COMPARISON OF CALCULATED AND EXPERIMENTAL THERMAL CONDUCTIVITIES

	temp °K	$\lambda \times 10^4$ J cm^{-1} sec^{-1} °C^{-1}			
		λ_H	λ_A(I)	λ_A(II)	$\lambda_{expt.}$
Ar	84·2	9·98	12·65	10·94	12·60
	87·3	9·38	12·22	10·47	12·16
N_2	69·1	10·37	12·84	11·21	15·11
	71·4	9·94	12·55	10·87	14·80
	77·3	8·58	11·48	9·75	13·96
CO	72·0	7·81	11·02	9·22	15·89
	77·7	6·71	10·28	8·43	15·05
	80·8	6·16	9·94	8·07	14·21
CH_4	93·2	17·36	20·67	18·34	21·53
	103·2	15·42	19·22	16·73	20·27
	108·2	14·52	18·57	16·01	19·64
C_6H_6	288·2	11·94	12·79	12·05	14·94
	298·2	11·50	12·40	11·62	14·63
	308·2	11·02	11·96	11·16	14·24
	318·2	10·58	11·57	10·74	13·89
CCl_4	298·2	10·20	10·67	10·23	10·64
	308·2	9·81	10·30	9·84	10·51
	318·2	9·45	9·97	9·49	10·39

previously given [1] with the exception of benzene which has been altered to take into account the results of Horrocks and McLaughlin.[10] Table 1 gives the experimental results, together with the values calculated on the harmonic approximation λ_H. These differ slightly from those previously given due to the use of the Wentorf, Buehler, Hirschfelder and Curtiss values of L_1 and M_1 in the present work. The effect of the change to the anharmonic frequency alone is denoted by λ_A(I) which still includes the harmonic specific heat, while λ_A(II) is the result obtained when both the anharmonic frequency and specific heat are used. Comparison of λ_A(I) and λ_A(II) shows that the correction for the anharmonic specific heat decreases the effect of including the anharmonic frequency alone. In general, however, there is better agreement between calculated and experimental values on the anharmonic model than was obtained in the harmonc approximation. As expected, the correction is greatest for the most expanded liquids like CO.

Better agreement is obtained between experiment and λ_A(I) which contains the specific heat as a constant multiple of k than the case λ_A(II) which includes a temperature and density dependent specific heat. This is also found when the experimentally determined value of the ratio of the viscosity to the thermal conductivity of the same series of liquids is examined in the form $m\lambda/k\eta$. For all the present liquids this is within about 10 % of the value 2·5 with a slight dependence on temperature whereas the ratio $m\lambda/C_v\eta$ produces no correlation when C_v is either the total or configurational specific heat.

As can be inferred from fig. 2, calculations using the pure quartic frequencies would be worse than the harmonic approximation. This case has only been included because of its use in examining the temperature dependence of thermal conductivity on the present model which is being investigated.

Thanks are due to the National Coal Board for the award of bursaries to A. F. C. and J. K. H.

[1] J. K. Horrocks and E. McLaughlin, *Trans. Faraday Soc.*, 1960, **56**, 206.
[2] J. K. Horrocks, E. McLaughlin and A. R. Ubbelohde, *Trans. Faraday Soc.*, 1963, **59**, 1001.
[3] E. McLaughlin, *Progr. in Int. Res. on Thermodynamic and Transport Properties* (Academic Press, New York, 1962) p. 288.
[4] J. K. Horrocks and E. McLaughlin, *Trans. Faraday Soc.*, 1963, **59**, 1709.
[5] J. E. Lennard-Jones and A. F. Devonshire, *Proc. Roy. Soc. A*, 1937, **163**, 53.
[6] R. H. Wentorf, R. J. Buehler, J. O. Hirschfelder and C. F. Curtiss, *J. Chem. Physics*, 1950, **18**, 1484.
[7] L. D. Landau and E. M. Lifschitz, *Mechanics* (Pergamon Press, London, 1960), p. 25.
[8] D. R. Hartree, *Numerical Analysis* (O.U.P., 1958), p. 115.
[9] E. T. Goodwin, *Proc. Camb. Phil. Soc.*, 1949, **45**, 241.
[10] J. K. Horrocks and E. McLaughlin, *Proc. Soc. A*, 1963, **273**, 259.

PRINTED IN GREAT BRITAIN AT
THE UNIVERSITY PRESS
ABERDEEN

MUTUAL DIFFUSION IN DENSE SUPERCRITICAL FLUIDS

By

D.J. McConalogue
Centre for Computing and Automation
IMPERIAL COLLEGE
LONDON, S.W.7

and

E. McLaughlin*
Department of Chemical Engineering
Louisiana State University, Baton Rouge, La.

*Permanent Address:

Department of Chemical Engineering and Chemical Technology
IMPERIAL COLLEGE
LONDON, S.W.7

Proofs to:

Dr. E. McLaughlin
Department of Chemical Engineering and Chemical Technology
IMPERIAL COLLEGE
LONDON, S.W.7

(ABSTRACT)

An expression of the mutual diffusion coefficient of a dense binary system of hard spheres is derived by using the Percus-Yevick approximation for the contact radial distribution function, together with Thorne's extension of the Enskog theory. The variation of the mutual diffusion coefficient with pressure, composition and the ratio of the molecular diameters is considered and applications are made to real systems.

I INTRODUCTION

In the study of transport properties of dense supercritical fluids attention has been restricted mainly to pure fluids. There is however a need for measurements on mixed supercritcal fluids, not only for their importance in practical systems, but also for use in testing theoretical models.

The present paper deals with the variation of the mutual diffusion coefficient of a dense gas mixture of different sized hard spheres as a function of pressure and composition. In addition an attempt is made to apply the results to mutual diffusion in real gas mixtures at high pressures.

II Mutual Diffusion in Hard Sphere Systems

In a recent paper[1] Thorne's extension[3] of the Enskog theory[2] of transport properties of dense hard sphere fluids has been used to obtain an expression for the mutual diffusion coefficient D of a dense gas binary mixture in terms of the corresponding dilute gas coefficient $\mathcal{D}$ at the same temperature.

The result can be written

$$\frac{nD}{\mathcal{N}\mathcal{D}} = \frac{(1-\xi)^2}{(1-\xi) + \frac{3r\xi}{(1+r)}\left\{\frac{x_1+x_2r^2}{x_1+x_2r^3}\right\}} \qquad (1)$$

The number density in the dense phase is n and that in the dilute phase $\mathcal{N}$ with $r = \sigma_{22}/\sigma_{11}$ the ratio of the molecular diameters of the two species. ξ is the ratio of the volume of the molecules to the volume of the system, i.e.

$$\xi = b_{11}^* + b_{22}^*$$

$$= \mathcal{V}_1^* (x_1 + x_2r^3)/\mathcal{V} \qquad (2)$$

where

$$b_{ii}^* = \frac{1}{6}\pi n_i \sigma_{ii}^3 \qquad (3)$$

and x_1 and x_2 are the mole fractions. $\mathcal{V}_1^*$ is the volume of a molecule of species 1 and $n = n_1 + n_2 = 1/\mathcal{V}$ where $\mathcal{V}$ is the volume of the system per molecule.

In deriving eq (1) use was made of the expression for the contact radial distribution function $g_{12}(\sigma_{12})$

$$g_{12}(\sigma_{12}) = \left[\sigma_{22}g_{11}(\sigma_{11}) + \sigma_{11}g_{22}(\sigma_{22})\right]/2\sigma_{12} \qquad (4)$$

where

$$g_{11}(\sigma_{11}) = \left\{ (1+\tfrac{1}{2}\xi) + \frac{3}{2}\,\frac{\pi \ln 2}{6}\,\sigma_{22}^{2}\,(\sigma_{11} - \sigma_{22}) \right\} (1-\xi)^{-2} \qquad (5)$$

with a corresponding expression for $g_{22}(\sigma_{22})$ with the species numbers interchanged. These equations were obtained by Lebowitz[4] from the Percus-Yevick approximation in the equilibrium theory of fluids. As the equation of state of systemoof hard spheres in three dimensions is not known exactly the pressure calculated from the approximate radial distribution function differs[5] depending on the route used for the derivation. When obtained via the compressibility equation

$$1-\sum_i n_i \int c_{ij}(R)\, d\underset{\sim}{R} = \partial p^c / kT \partial n_j \qquad (6)$$

the result for a binary mixture on using eq(4) gives for the pressure p^c

$$\frac{p^c v_1^*}{RT} = \frac{\xi(1+\xi+\xi^2)}{(1-\xi)^3(x_1+x_2\gamma^3)} - \frac{3x_1x_2(1-\gamma)^2\xi^2\left[(1+\gamma)+\gamma\xi\left(\frac{x_1+x_2\gamma^3}{x_1+x_2\gamma^2}\right)\right]}{(x_1+x_2\gamma^3)^2(1-\xi)^3} \qquad (7)$$

c_{ij} the direct correlation function is related in the Percus-Yevick approximation to the radial distribution function $g_{ij}(R)$ and the intermolecular potential $\phi_{ij}(R)$ by the equation

$$g_{ij}(R)\left[\exp\left\{-\phi_{ij}(R)/kT\right\} - 1\right] = \exp\left\{-\phi_{ij}(R)/kT\right\} c_{ij}(R) \qquad (8)$$

Alternatively when ξ obtained via the virial theorem

$$p^{v}/kT = \sum_i n_i - \frac{2}{3}\pi \sum_{ij} n_i n_j \int R^3 \phi'_{ij}(R) g_{ij}(R)\, dR \qquad (9)$$

the pressure p^{v} is given by

$$\frac{p^{v}\mathcal{V}_1^*}{kT} = \frac{p^{c}\mathcal{V}_1^*}{kT} - \frac{3\xi^4}{(1-\xi)^3}\left\{\frac{x_1+x_2r^2}{x_1+x_2r^3}\right\}^3. \qquad (10)$$

If the correct radial distribution function was known then

$p^{v} = p^{c} = p$

In order to evaluate eq (1) at various constant pressures at a fixed temperature the value of ξ must be found from either eq (7) or eq (10). For the pure fluid[6] the pressure obtained from the compressibility equation is closer to the machine calculations for an assembly of hard spheres than that obtained from the virial equation. However, in what follows the results for both cases are considered.

Values of $nD/\mathcal{D}$ as a function of x_1 were calculated for

$r = \frac{1}{5}, \frac{1}{3}, \frac{1}{2}, \frac{2}{3}, 1, \frac{3}{2}, 3$ and 5 at $p\mathcal{V}_1^*/kT = 1, 2, 4, 8, 20$

and 30. These results were obtained by fixing r and $p\mathcal{V}_1^*/kT$ and solving eqs(7) and (10) numerically on a computer to give ξ for a fixed x_1 and r. Where overlap occurs between the present calculations for ξ and those of Lebowitz and Rowlinson[5] a check showed that at constant pressure the reduced excess volumes $\mathcal{V}_e/\mathcal{V}_1^*$ are in exact agreement. The excess volume per molecule is defined by

$$\mathcal{V}_e = \mathcal{V} - x_1\mathcal{V}_1^o - x_2\mathcal{V}_2^o \qquad (11)$$

with $\mathcal{V}_1^o$ and $\mathcal{V}_2^o$ the volumes per molecule of pure systems composed of species 1 and 2 respectively.

Figure 1 gives a representative set of curves for the variation of $nD/n\mathcal{D}$ as a function of $p^c\mathcal{V}_1^*/kT$ for r=0.5 at x_1=0, 0.5 and 1. These results reflect the expected behaviour of a monotonic decrease with increasing pressure. It should be remembered however that ξ and n are related by eq(2) and hence $D/\mathcal{D}$ will drop faster than $nD/n\mathcal{D}$. Results have been left in the latter form for convenience in identifying the common low pressure limit. Fig. 2, gives the variation of $nD/n\mathcal{D}$ with composition for a series of

Table 1. Comparison of $nD/n\mathcal{D}$ values obtained from the compressibility (1) and virial pressures (2).

$p\mathcal{V}_1^*/kT = 1$

x_1	0	0.2	0.4	0.6	0.8	1.0	
r = 1/5	0.9732	0.7823	0.6945	0.6494	0.6229	0.6056	(1)
	0.9732	0.7819	0.6923	0.6450	0.6167	0.5979	(2)
r = 3/2	0.3127	0.3235	0.3377	0.3569	0.3844	0.4266	(1)
	0.2914	0.3040	0.3202	0.3419	0.3724	0.4182	(2)

$p\mathcal{V}_1^*/kT = 20$

x_1	0	0.2	0.4	0.6	0.8	1.0	
r = 1/5	0.6958	0.2814	0.2447	0.2315	0.2247	0.2206	(1)
	0.6952	0.2534	0.2076	0.1904	0.1815	0.1760	(2)
r = 3/2	0.0718	0.0743	0.0777	0.0825	0.0900	0.1033	(1)
	0.0434	0.0461	0.0497	0.0549	0.0630	0.0775	(2)

r ratios at $p^c v_1^*/kT = 4$. Obviously when r=1 the pressure and ξ are independent of composition as can be seen from eqs (7), (10) and (2) hence D as in the dilute gas is composition independent. As shown previously[1] the present expression for D in this case, then reduces to the result of Longuet-Higgins, Pople and Valleau,[7]

$$D = \frac{\sigma}{4}\left\{\frac{\pi kT(m_1+m_2)}{2m_1m_2}\right\}^{\frac{1}{2}}\left(\frac{p}{nkT}-1\right)^{-1} \qquad (14)$$

In principle it should be possible to obtain diffusion coefficients of mixed systems of hard spheres using Monte Carlo type calculations. None are however available, but it would be of interest to see if those calculated using p^c were better than those from p^v. Table 1 gives values of $nD/n\mathcal{D}$ for pv_1^*/kT = 4 and 20 for r = $\frac{1}{5}$ and $\frac{3}{2}$. The first line at each r value was obtained using ξ from $p^c v_1^*/kT$ and the second from $p^v v_1^*/kT$. As expected differences are less at the lower pressure.

III Application to Real Fluids

In view of the experimental difficulties involved, measurements of diffusion coefficients in mixtures of dense supercritical gases are rather scarce. Results have been obtained by Jeffries and Drickamer[8] on CO_2(1) - CH_4(2) mixtures at two compositions $x_1 = 0.5$ and 0.75 which can be used to compare with eq (a). This is done for the 25°C results.

Hard sphere diameters for CO_2 and CH_4 were obtained by equating the experimental $\mathcal{D}$ for CO_2 - CH_4 mixtures at 1 atmosphere to the Chapman-Enskog expression for the mutual diffusion coefficient of a dilute gas of hard spheres

$$\mathcal{D} = \frac{3}{8n\sigma_{12}^2}\left\{\frac{kT(m_1+m_2)}{2\pi m_1 m_2}\right\}^{\frac{1}{2}} \qquad (13)$$

which is composition independent in the first approximation. This gives σ_{12} and hence σ_{22} after obtaining σ_{11} from the corresponding self-diffusion coefficient of CO_2 measured by Amdur, Irvine, Mason and Ross[10] together with the equations

$$\mathcal{D}_1^{\circ} = \frac{3}{8n\sigma_{11}^2}\left\{\frac{kT}{\pi m_1}\right\}^{\frac{1}{2}} \qquad (14)$$

and

$$\sigma_{12} = \tfrac{1}{2}(\sigma_{11}+\sigma_{22}) \qquad (15)$$

With these σ's and the ratio n/n from the density data of Sage, Lacey, Reamer and Olds eq (1) can be calculated for various pressures. This proceedure is equivalent to fitting eq (1) at 1 atm, and comparison between calculated and experimental results at pressures between 40 and approximately 200 atms given in fig 3 shows that the model does give the essential features of the experimental results viz a diffusion coefficient which falls rapidly with increasing pressure and that at a particular fixed pressure the $x_1 = 0.75$ isotherm is below that for $x_1 = 0.5$. Although of the correct order of magnitude however agreement between the calculated and experimental D's is not good but this of course would have been anticipated, as in applying the Enskog theory to one component dense gas properties 'two point fitting' is necessary to obtain satisfactory agreement between calculated and experimental transport properties. For example for

the case of viscosity η, the Enskog equation is fitted at the dilute gas end and at the minimum in the η/ϱ curve where ϱ is the density of the fluid.

In order to demonstrate that this can be done for binary dense gas diffusion we use the experimental results of Durbin and Kobayashi[12] who measured the self-diffusion coefficient of Kr-85 in a series of gases at pressures from atmospheric to 400 atm.

While $\mathscr{D}$ is independent of x, D for the dense fluid varies with x. At the extreme ends of the composition range we adopt the following notation for D:

$$D = D_2^{\infty 1} \qquad\qquad D = D_1^{\infty 2}$$

$$1 \text{tx}_1 \rightarrow 1 \qquad\qquad 1 \text{tx}_1 \rightarrow 0$$

and by choosing Kr-85 as species 2 we can re-write eq 1 in the form

$$\frac{nD_2^{\infty 1}}{\mathscr{D}} = \frac{(1-b^*)^2}{(1-b^*)+3b^*\frac{r}{1+r}} \qquad (16)$$

where $b^* = \frac{1}{6}\pi n\sigma_{11}^3$ as species 2 is present only in vanishingly small concentrations. σ_{12} was obtained from the experimental[11] 1 atm $\mathcal{D}$ values for the various systems and σ_{22} from the 1 atm $\mathcal{D}_2^{\circ}$ values as before, so that eq. 16 fits the low-pressure data. Using the value of σ_{11} only, b* was calculated from the appropriate density data, and r/1+r taken as a disposable parameter obtained by fitting eq. (16) to the experimental $D_2^{\infty 1}/\mathcal{D}$ at a higher pressure. With this value of r/1+r the other values of $D_2^{\infty 1}/\mathcal{D}$ over the pressure range were calculated. The results are shown in fig. 4 for Kr-85 diffusing in dense supercritical argon

TABLE 2 Comparison of calculated and experimental self-diffusion coefficients of Kr-85 in various dense gases at 35°C

Kr - CO_2			Kr - N_2			Kr - C_2H_4		
patm	$D_2^{COl} \times 10^3$ $cm^2 sec^{-1}$		patm	$D_2^{COl} \times 10^3$ $cm^2 sec^{-1}$		patm	$D_2^{COl} \times 10^3$ $cm^2 sec^{-1}$	
	calc.	exp.		calc.	exp.		calc.	exp.
5.765	20.43	20.47	17.88	8.94	8.85	13.69	7.70	7.98
13.66	8.32	8.41	24.55	6.52	6.59	30.25	3.04	3.18
21.55	5.17	5.05	34.93	4.60	4.71	45.80	1.65	1.82
30.36	3.49	3.49	69.33	2.36	2.44	62.07	1.07	0.98
*43.80	2.25	2.25	135.74	1.28	1.29	70.07	0.58	0.64
57.48	1.56	1.54	*203.8	0.92	0.92	* 79.94	0.50	0.50
57.89	1.54	1.52	273.5	0.75	0.72	89.46	0.48	0.45
			339.7	0.67	0.63	112.12	0.47	0.38
			408.4	0.62	0.55			

*denotes high pressure value at which fitting of eq. (16) was made

and for purposes of comparison the calculated curve obtained by using r from the σ's obtained from the dilute gas $\mathcal{D}$ and $\mathcal{D}_2^o$ as was done for the CO_2 - CH_4 mixtures is included. As expected, both methods are not very different at low pressures but at high pressures fitting r/1+r to the experimental $D_2^{col}/\mathcal{D}$ at one fixed high pressure value, in this case 324 atm, satisfactorily reproduces the values of the diffusion coefficient for the other pressures.

The degree of this agreement is illustrated in Table 2 for trace amounts of Kr-85 diffusing in nitrogen, carbon-dioxide and ethylene at high pressures where calculated and experimental coefficients are seen to agree on average within 5% over the pressure range. This is possibly close to the experimental accuracy of the results.

One of us, E.McL., wishes to thank the National Science Foundation for the award of a Senior Foreign Scientist Fellowship during which the major portion of this work was

completed. Thanks are also due to the faculty, particularly Professors J. Coates and P. Murrill of the L.S.U. Chemical Engineering Department at Baton Rouge, for their hospitality, and to Mr. A. de Souza for initial help with the computation.

1. E. McLaughlin (J. Chem. Phys. in the press)

2. S. Chapman and T.G. Cowling, "The Mathematical Theory of Non-uniform Gases", C.U.P. 2nd Edition, 1953, p.273 et seq.

3. H.H. Thorne quoted in ref. 2, p.292 et seq.

4. J.L. Lebowitz, Phys. Rev., 1964, 133 A895

5. J.L. Lebowitz and J.S. Rowlinson, J. Chem. Phys., 1964, 41, 133.

6. J.S. Rowlinson, Rep. Prog. Phys., 1965, 28, 169.

7. H.C. Longuet-Higgins, J.A. Pople and J.P. Valleau, "Transport Processes in Statistical Mechanics" 73 (1958), Interscience Publishers, London.

8. Q.R. Jeffries and H.G. Drickamer, J. Chem. Phys., 1954, 22, 436.

9. International Critical Tables, 1929, 5, 62. McGraw-Hill, New York.

10. I. Amdur, J.W. Irvine, E.A. Mason and J. Ross, J. Chem. Phys., 1952, 20, 436

11. B.H. Sage, W.N. Lacey, H.H. Reamer and R.H. Olds, Ind. Eng. Chem., 1944, 36, 88.

12. L. Durbin and R. Kobayashi, J. Chem. Phys., 1962, 37, 1643.

Figure 1. Variation of $nD/n_2^{\ominus}$ with $p^c v_1^*/kT$ for $r = 0.5$, $x_1 = 0$, 0.5 and 1

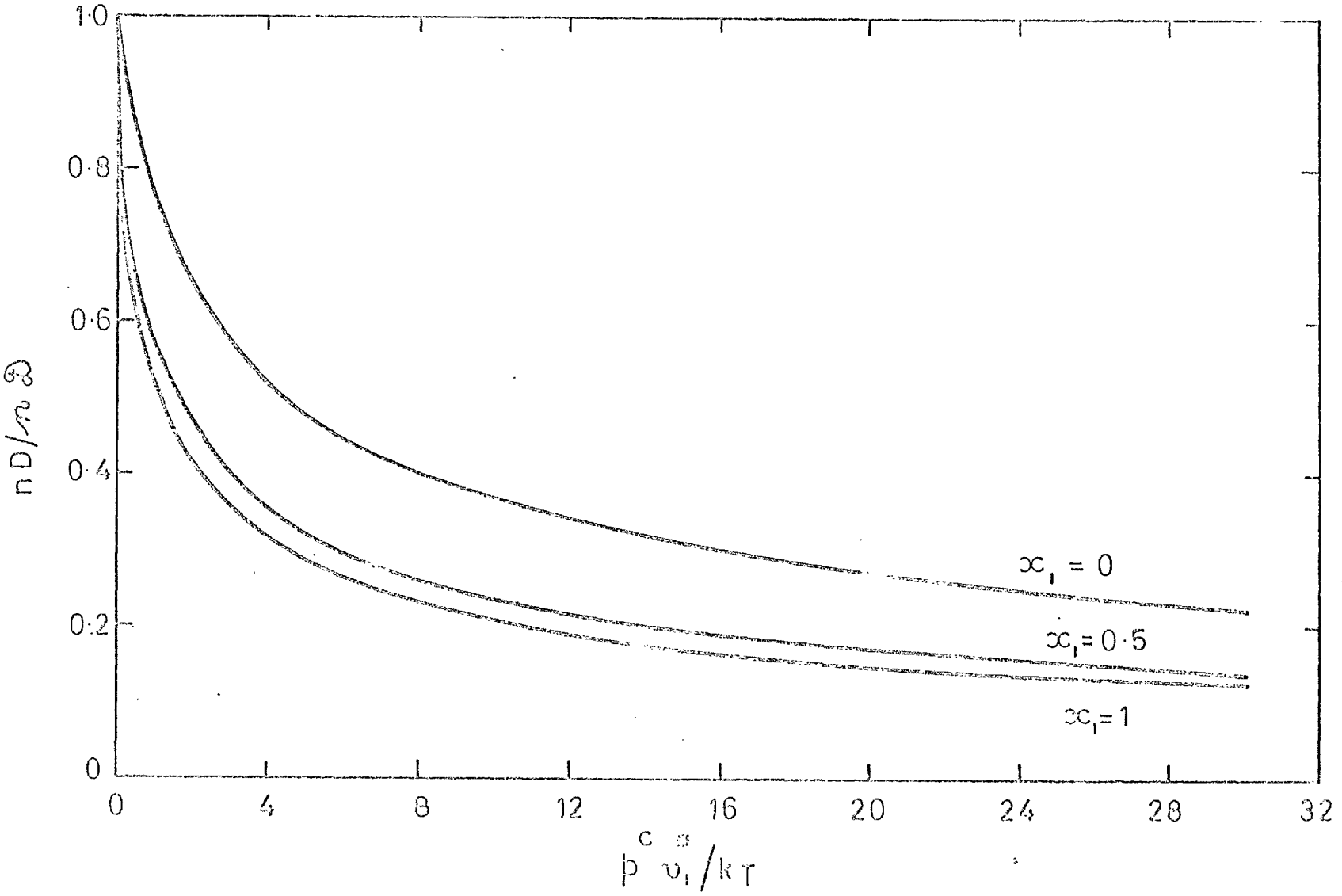
1·0
0·8
0·6
0·4
0·2
0
nD/nD
0
4
8
12
16
20
24
28
32
$p^c \tilde{v}_1/kT$
$x_1 = 0$
$x_1 = 0·5$
$x_1 = 1$

Figure 2. Variation of $nD/\mathscr{D}$ with x_1 for various values or r at $p^c v_1^*/kT = 4$

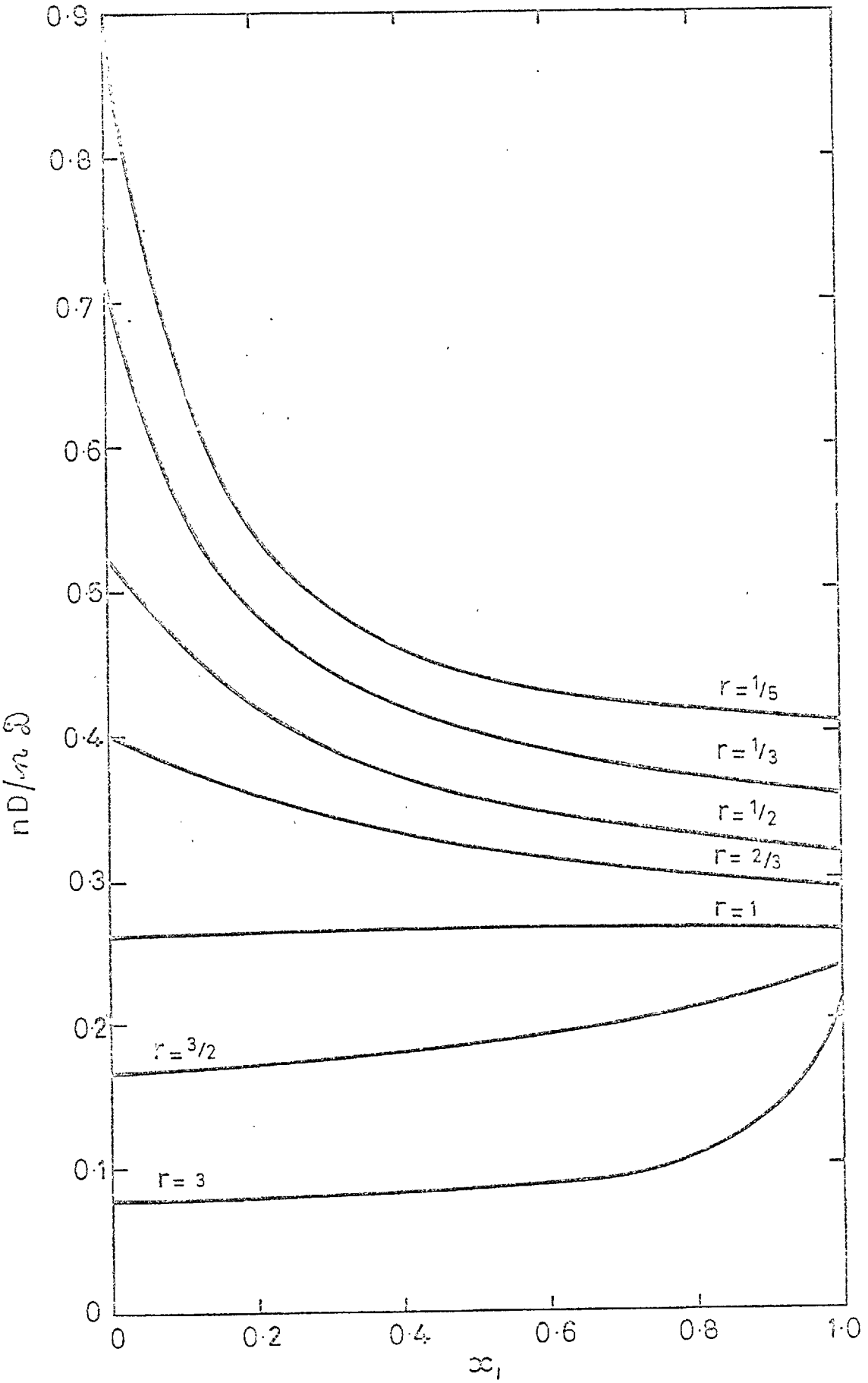
0·9
0·8
0·7
0·6
0·5
0·4
0·3
0·2
0·1
0
nD/nΩ
r = 1/5
r = 1/3
r = 1/2
r = 2/3
r = 1
r = 3/2
r = 3
0
0·2
0·4
0·6
0·8
1·0
x1

Figure 3. Variation of D with pressure for the system CO_2-CH_4 at 25°C for mole fractions of CO_2 of o.5 and o.75. Dotted lines, calculated, solid lines, experimental.

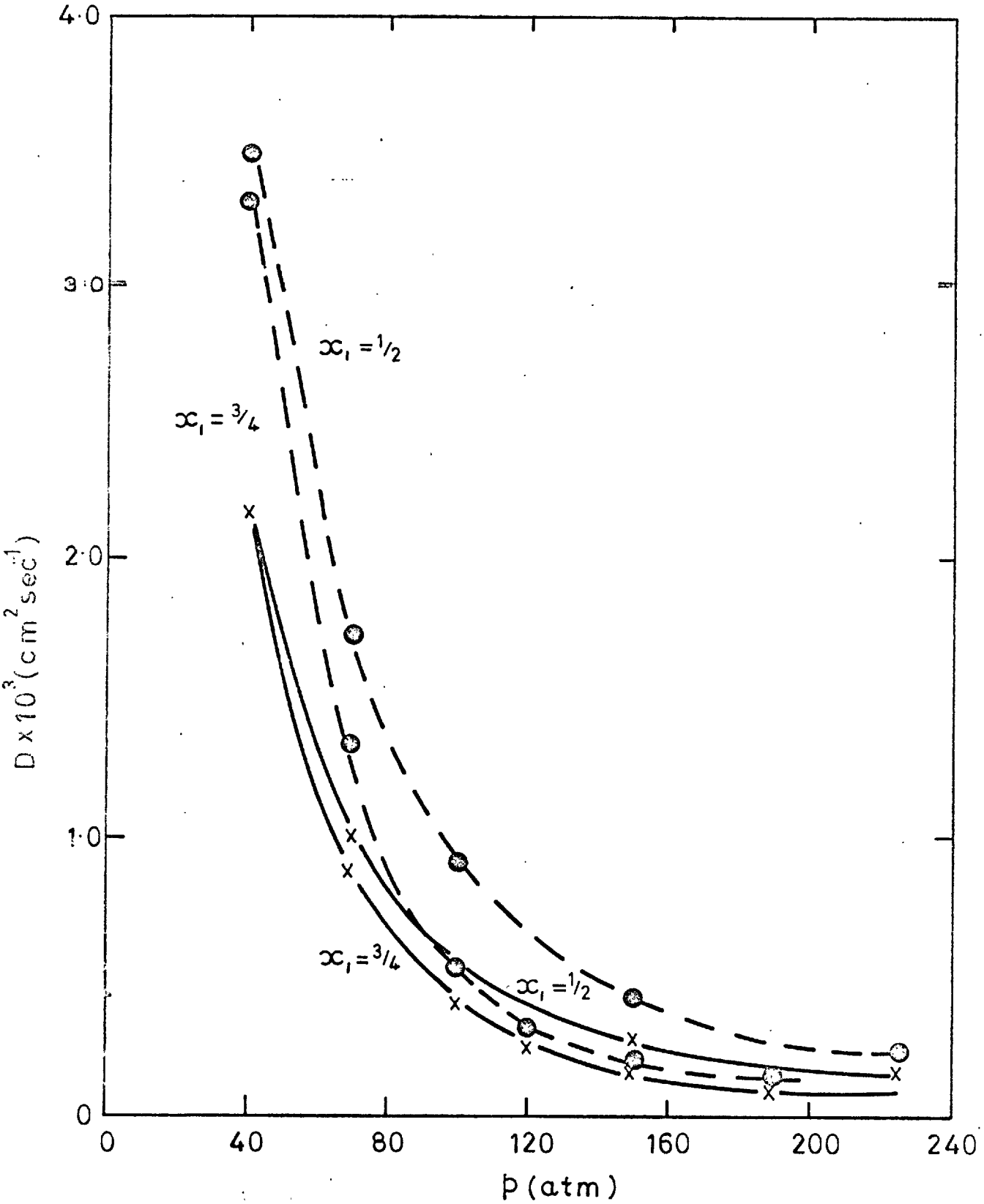
4·0
3·0
2·0
1·0
0
0
40
80
120
160
200
240
D x 10³ (cm² sec⁻¹)
P (atm)
x₁ = 1/2
x₁ = 3/4
x₁ = 3/4
x₁ = 1/2

Figure 4. Variation of log ($D_2^{001} \times 10^3/\mathcal{D}$) with pressure for the self-diffusion coefficient of Kr 85 in argon at 35°C. Open circles indicate experimental results. The broken curve is obtained from calculated values using dilute gas data, and the solid curve values calculated using dilute gas and one high pressure point.

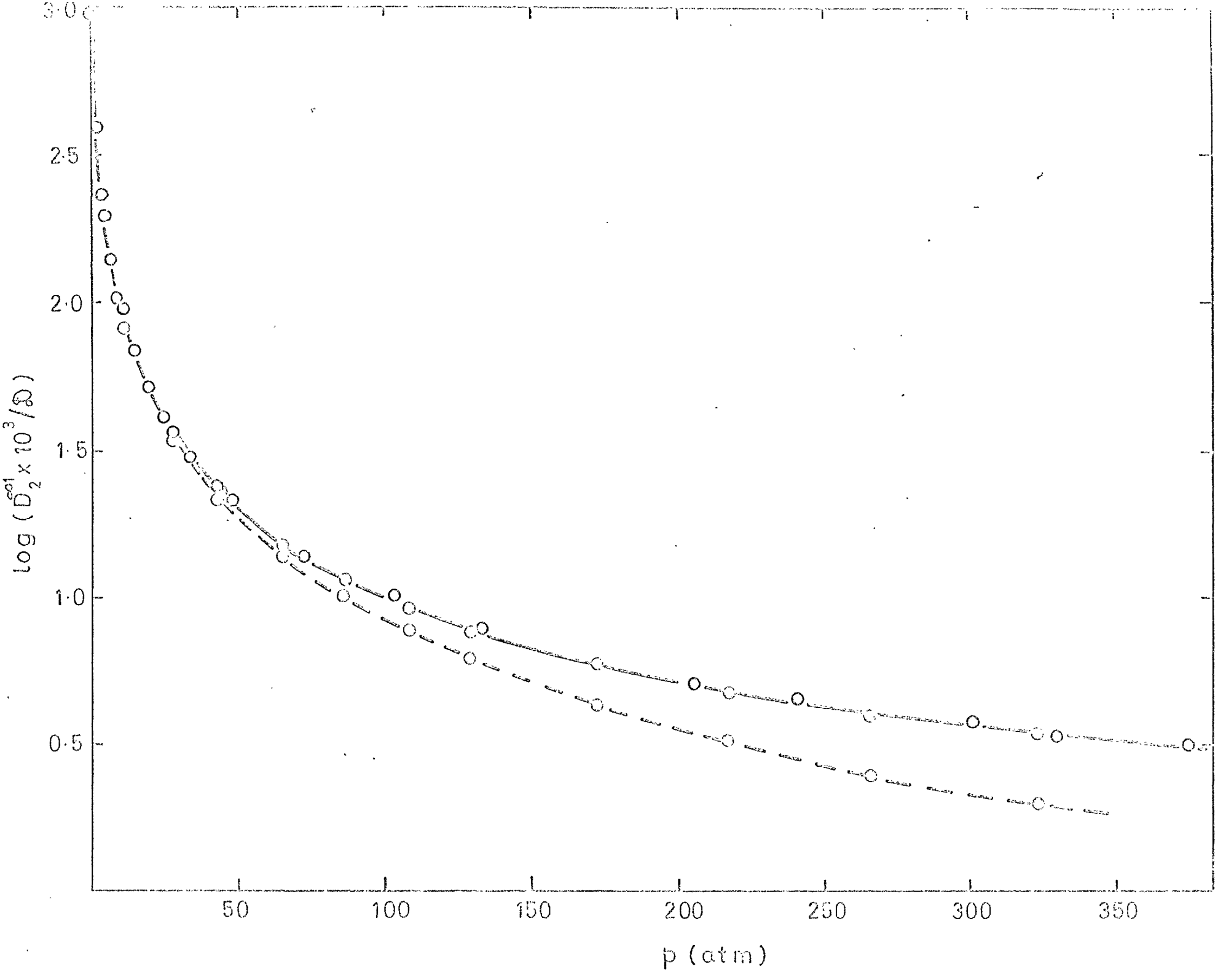
3·0
2·5
2·0
1·5
1·0
0·5
log ($D_2^{\infty 1} \times 10^3 / \Omega$)
50
100
150
200
250
300
350
p (atm)